# 4 Mechanical Aspects on EOCBs

## 4.1 Introduction

Introduced in chapter 2 and 3, our group has developed a new EOCB fabrication technology (patent pending) based on casting of thermal addition curing of two-component silicone rubber: PDMS (polydimethylsiloxane). This material has outstanding optical, thermal, and mechanical properties, an extremely favorable price (50 €/ l) and low shrinking (< 0.3 %) during polymerization. However, three critical points exist in PDMS based EOCB fabrication and products qualities. First it is the bonding quality between core and cladding, then cladding and cladding layer and the last is between two cladding layers and general PCB substrates (See Fig. 4.1). It is vital for the reliable operation of EOCBs to realize mechanically stable interfaces between core and cladding layers, cladding layers and the whole optical PDMS layers and the adjacent PCB substrate materials like FR4, Kapton and copper coated boards etc. In case of bubbles and insufficient interfacial adhesion among them, thermal stress due to CTE (Coefficient of Thermal Expansion) and Young's modulus mismatch will lead to delamination and resulting damage of the boards.

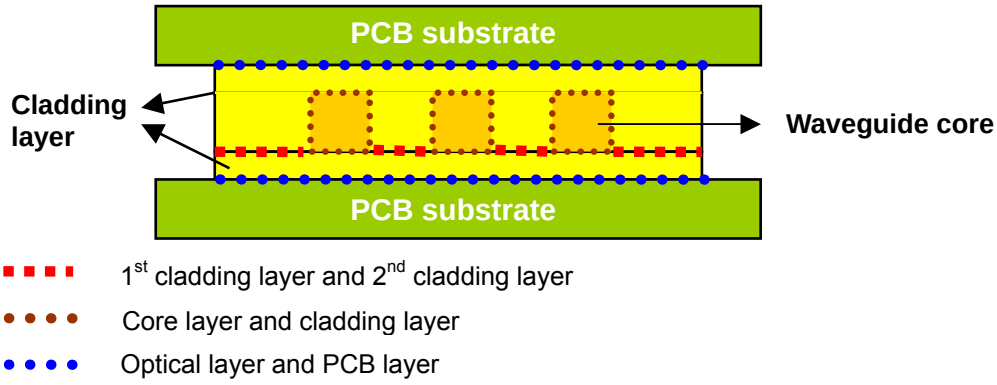


**Fig. 4.1** *Basic structure of EOCB and mechanically critical interfaces*

The actually used two-component PDMS prepolymer is well known for its reluctance to adhere to most of the substrates including cured PDMS surfaces. [69] Unfortunately this property prevents the realization of self-packaged EOCBs. To overcome this problem and to achieve good adhesion between PDMS and PDMS, and PDMS and general PCB substrates applied in EOCB packaging appropriate curing conditions for core and cladding PDMS prepolymer are identified and special Surface-Adhesion-Promoters (SAP) have been developed both based on the researches on PDMS curing mechanism. In addition, the used PCB substrates are studied respectively from molecular to topography and various compatible treatment methods to these substrates are also developed in terms of the SAP molecular structural properties. By applying this procedure, we achieved – in one fabrication step - perfect curing of the liquid PDMS prepolymer without bubbles, although staying in contact with packaging substrates, as well as a good bonding between boards and PDMS layers. After curing, the well integrated PDMS optical layer is automatically laminated and packaged by two PCB carriers resulting in real-sense self-packaged EOCBs.

## 4.2 Curing Mechanism of Polydimethylsiloxane

Most biomolecular chemical reactions can be adapted to produce cross-linking provided the molecules are designed to form a three dimensional network as a result of the cross-linking reaction i.e., at least one of the molecules must be trifunctional. Given the relative ease with which organic functionalities can be attached as side chains to a polysiloxane backbone one would expect some adaptation of conventional organic cross-linking chemistries to be applied to the problem of cross-linking siloxanes. For these chemistries to be useful it is essential that the desired reaction occurs as expected when the organic functionalities are attached on the polymer, and the resulting cross-link should not impair the predominantly siloxane characteristics of the material.[70]

However, because silicon is such a strong eletropositive element its position relative to the organic substituent is critical in terms of the behavior of the attached orgainc substituent. Thus an organic substituent placed on the carbon β to the silicon can, because of the so-called β-effect, participate in totally unexpected reactions. The general effect of silicon substitution on an organic functional group can be illustrated by the effect of tri-methyl silyl substitution on the acidity of aliphatic carboxylic acids. The electron donating effect of the tri-methyl silyl group tends to weaken the acid and this effect is not lost until there are three carbons

between the silicon and the carboxy group. A similar pattern is observed in substituted aliphatic amines, although in the case the tri-methyl silyl group increases the basicity of the amine. Thus in general a reactive organic substituent must be located at least three carbons away from the silicon in order to preserve its normal reaction behavior.[71]

It is clear that each cross-link would contain a large number of methylene and other groups which would introduce a significant degree of organic character to the resulting cross-linked material, especially when the number of functional groups is optimized to give the degree of cross-linking needed to produce the desired physical properties and acceptable cure times. Thus it is clear that the siloxane character of the material would be significantly impaired if this or similar reactions were used as the cross-linking reactions. These reactions, therefore, tend to find utility where the intention is to modify the properties of organic materials by the incorporation of siloxanes, where additional organic character is not a problem, or in the formation of siloxane organic-copolymers.

Thus the cross-linking reactions, which will be described in more detail, are those which leave the siloxane properties virtually unchanged and produce materials, usually rubbers and coatings, which retain the desirable properties of the polydimethysiloxanes, namely their thermal and chemical stability and their ability to remain flexible at low temperature.

There are four classes of reaction which are widely used to cross-link siloxanes in commercial applications: [70]

1. Peroxide-induced free radical reactions
2. Condensation reactions
3. Hydrosilylation addition reactions
4. Hydridosilane/ silanol reaction.

In my thesis, it is mainly focused on PDMS based polymers and hydrosilylation addition reactions.

### 4.2.1 Hydrosilylation Addition Reactions in PDMS Materials

The Si-H bond is polar, long, and weak, and therefore, very reactive. [70] Its addition across a double bond (hydrosilylation) is an important reaction not only in organosilicon chemistry but also in organic synthesis and dendrimer and polymer chemistry. The hydrosilylation reaction, which involves the addition of a silicon

hydrogen (SiH) bond to an unsaturated carbon carbond bond, catalytzed by a noble metal, typically e.g. Pt is a well-known and versatile reaction in organosilicon chemistry. Additionally it has been widely used in the synthesis of organofunctional siloxanes and in the cross-linking of siloxane polymers. Many studies have been devoted to the soluble platinum catalyzed hydrosilylation reaction (eq. 4.1) since its discovery by speier in the late 1950. Industrially, the reaction is employed in the synthesis of silane coupling agents and UV screeners. It is also utilized in the formation of three-dimensional networks from the crosslinking reaction of multifunctional silicone hydride polymers with multifunctional silicon vinyl polymers. Product applications include silicone rubbers, liquid injection molding compounds, paper release coatings, and pressure sensitive adhesives etc.[66, 70]

$$\text{″}\ Si - H + CH_2 = HC - Si\ \text{″} \quad \xrightarrow[T^oC,\ t]{Pt\ catalyst} \quad \text{″}\ Si - CH_2 - CH_2 - Si\ \text{″} \qquad (4.1)$$

Hydrosilylation reaction is a catalytic reaction for which a large variety of catalysts is available. They control the regio- and stereoselectivity including the enantioselectivity. Most of these catalysts operate according to the well established Chalk-Harrod mechanism or one of its variants resulting in the cis addition of a Si-H bond to an alkene. The Chalk-Harrod mechanism is the most commonly accepted mechanism for platinum-catalyzed hydrosilylation. In the classical Chalk-Harrod mechanism of olefin hydrosilylation a Si-H bond adds oxidatively to the metal atom of an olefin complex (Fig. 4.2). Migration of the hydride ligand onto the coordinated olefin generates the silyl alkyl intermediate, which undergoes reductive elimination to form the Si-C bond of the product. Normally, reactions following Chalk-Harrod-type mechanisms are accompanied by isomerization and scrambling of deuterium labels.[72-74]

In PDMS curing, the silyl (SiH) groups of the crosslinker reacted with vinyl groups through the hydrosilylation reaction. Simultaneously, but at a much slower rate, SiH groups are consumed through secondary crosslinking reactions that occur between SiH and SiOH groups newly-formed by the hydrolysis of SiH groups. (Some SiH groups might also react with chemical functionalities existing on the surface of the substrate.) These secondary reactions are favored when an excess of SiH over vinyl functionalities is used, and mainly occur after the completion of the primary hydrosilylation reaction. In this chapter, we will refer to the hydrosilylation reaction as the "crosslinking reaction" and to the secondary reactions that consume SiH as "post-cure reactions".

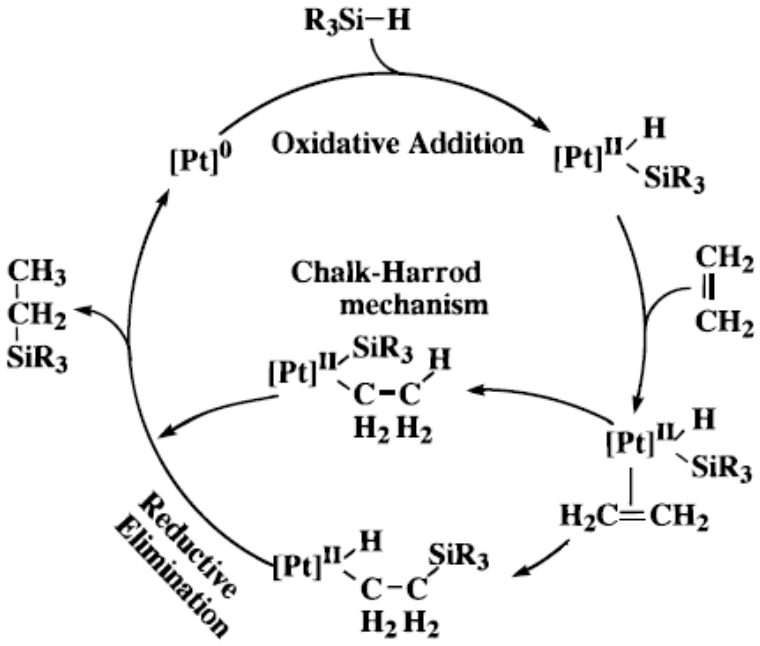


**Figure 4.2** *Chalk-Harrod mechanism of olefin hydrosilylation*

The nature and concentration of both the catalyst and the inhibitor, as well as the concentration of vinyl and SiH groups influence the reaction rate. At high temperature (ca. 70 °C) with a catalyst concentration of 50 ppm (Pt), the hydrosilylation crosslinking reaction is completed within tenths minutes.

Thereby, secondary reactions also occur, when they are favored with an excess of crosslinker and in the so-called "post-cure" stage and it has been verified experimentally through blending Si-H groups containing polysiloxane, Pt catalyst and water together. The mechanism of this reaction first requires the catalyzed hydrolysis of SiH groups:

$$\equiv Si - H + H_2O \xrightarrow[T^oC,\ t]{Pt\ catalyst} \equiv Si - OH + H_2 \uparrow \qquad (4.2)$$

One of crosslinking reactions in the stage is the condensation of two silanol groups (which are created in reaction 4.2):

$$\equiv Si - OH + OH - Si \equiv \xrightarrow{T^oC,\ t} \equiv Si - O - Si \equiv + H_2O \qquad (4.3)$$

The other type of crosslinking reaction occurs in this post-cure stage via the creation of Si-O-Si bonds, when the newly-formed silanol groups (SiOH) catalytically react with remaining SiH groups:

$$\text{″}\ Si - H + OH - Si\ \text{″} \xrightarrow[T^{o}C,\ t]{Pt\ catalyst} \text{″}\ Si - O - Si\ \text{″} + H_2 \uparrow \qquad (4.4)$$

The platinum-catalysed reactions 4.2 and 4.4 are much slower than the primary crosslinking reaction shown in Eq. 4.1. It is expected that the silanol condensation reaction (Eq. 4.3) is even slower than the SiH reactions (Eq. 4.2 and 4.4). Reactions shown in Eq. 4.2, 4.3 and 4.4 are jointly referred to herein as "post-cure reactions" as they occur when the system is allowed, or forced, to proceed towards its complete conversion rate.

### 4.2.2 Experimental Characterization to PDMS Curing

Introduced above, the hydrosilylation reaction of SiVi with a hydrosilane polysiloxane crosslinker creates a three-dimensional network. The rate of the reaction is a complex function of the curing temperature, catalyst nature and concentration, of inhibitor nature and concentration, and on the concentration of vinyl and SiH groups etc. For instance, RT 601 PDMS material, applied as waveguide cladding material in the thesis, under that conditions of 50 ppm (Pt) and in 1mm thick they can be completely cured within 5 min at 150 °C instead of 25 min at 70 °C. In details, the influences on rate of the reaction from catalyst concentration (Wacker EP), inhibition concentration (PT 88) and the concentration of base component and crosslinker were experimental investigated and illustrated below respectively in Fig. 4.3.

From these results, it is clear that platinum catalyst can improve PDMS curing evidently even if in quite few amounts. Then the presence of platinum will inversely affect the optical properties of the transparent PDMS system explained in Chapter 3 due to scattering of platinum colloid created by the extra Pt catalyst and medium sized molecular chain with uncrosslinked Si-Viny groups, so its concentrations should be controlled in one relatively low level. Inhibitor, organic temporal platinum catalyst deactivator, which can inhibit the quick curing due to its temporal deactivation and inhibition to platinum catalyst at room temperature, and it is helpful to extent the pot life of silicone rubber resins. When PDMS is thermally cured, the inhibitor will be evaporated as well and no extra influences on PDMS physical and chemical performances. Thus in the waveguide fabrication part, influences of concentrations of Si-H and Si-CH=$CH_2$, and temperature on PDMS curing will be investigated and studied as main points.

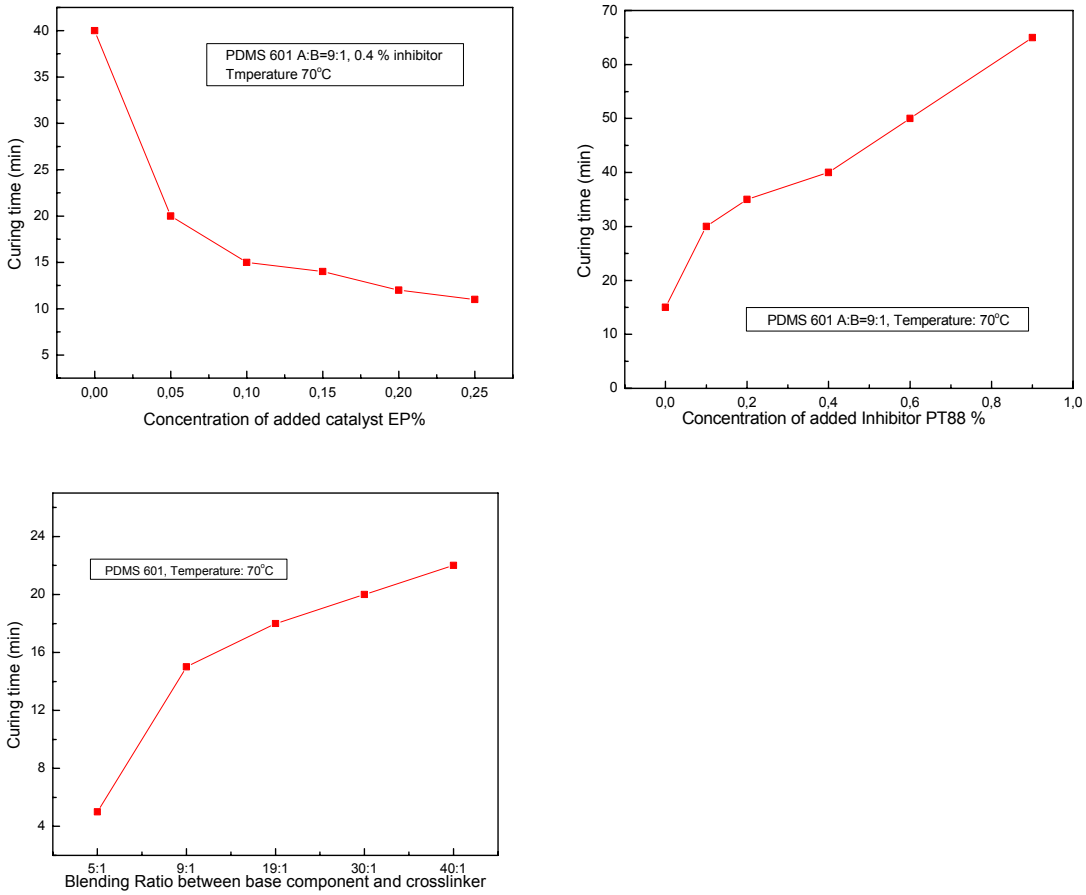


**Figure 4.3** *Various influences factors on PDMS curing*

Actually, the conversion of Si-H and Si-CH=$CH_2$ bonds can be followed and monitored by infrared and Raman spectroscopies. The IR and Raman spectra of RT 601 PDMS base component (compound A), crosslinker (compound B) and the corresponding cured polymer with different blending ratio are shown in Figure 4.3 respectively. From these spectra, the absorbances of the Si-H and Si-CH=$CH_2$ bonds (2159 and 1597 $cm^{-1}$, respectively) are nicely isolated peaks and may be applied for determination of state of curing of PDMS, because the Si-$CH_3$ absorbance (1263 $cm^{-1}$) will remain the same throughout the reaction and can act as an internal standard. The results are listed in Table 4.1.

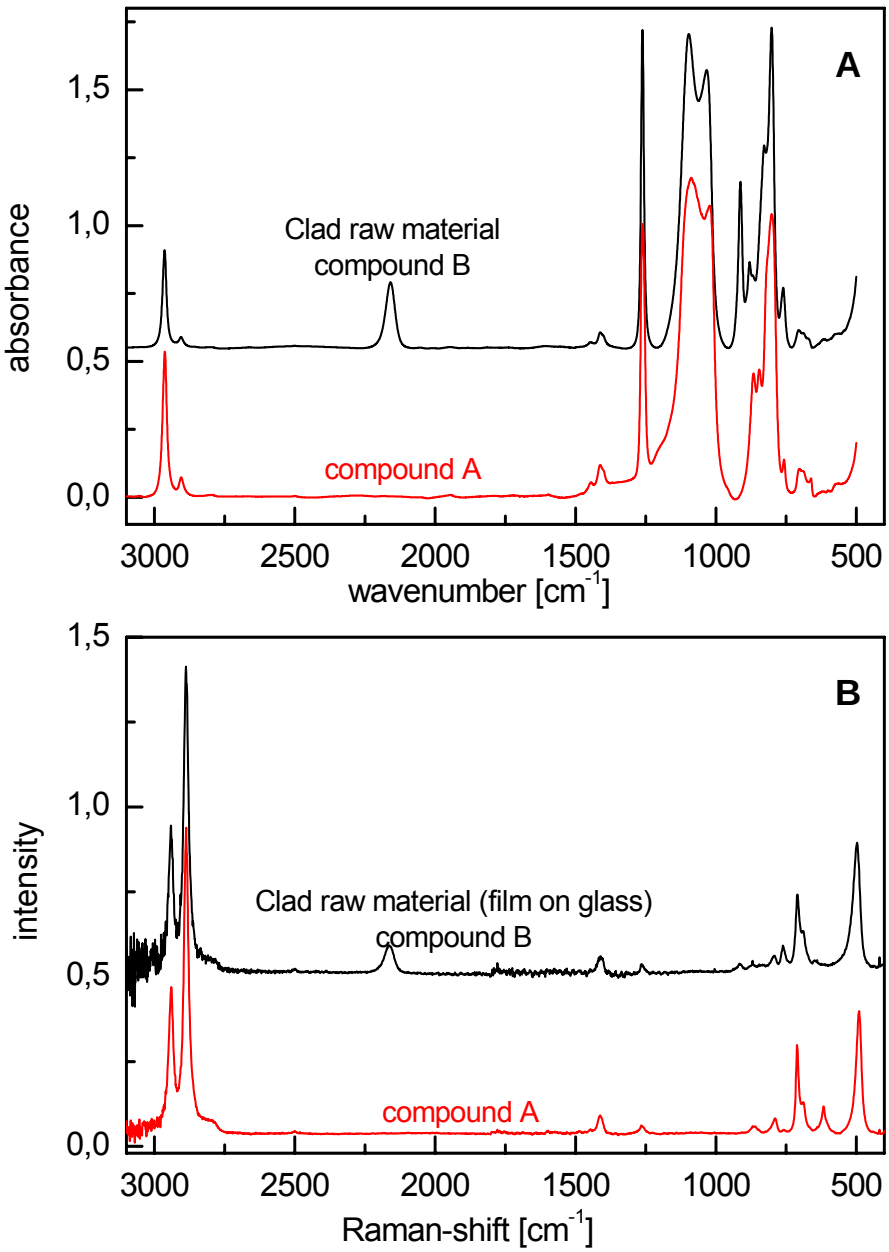


**Figure 4.4A** *FT-IR and FT-Raman spectra of PDMS prepolymers (cladding)*

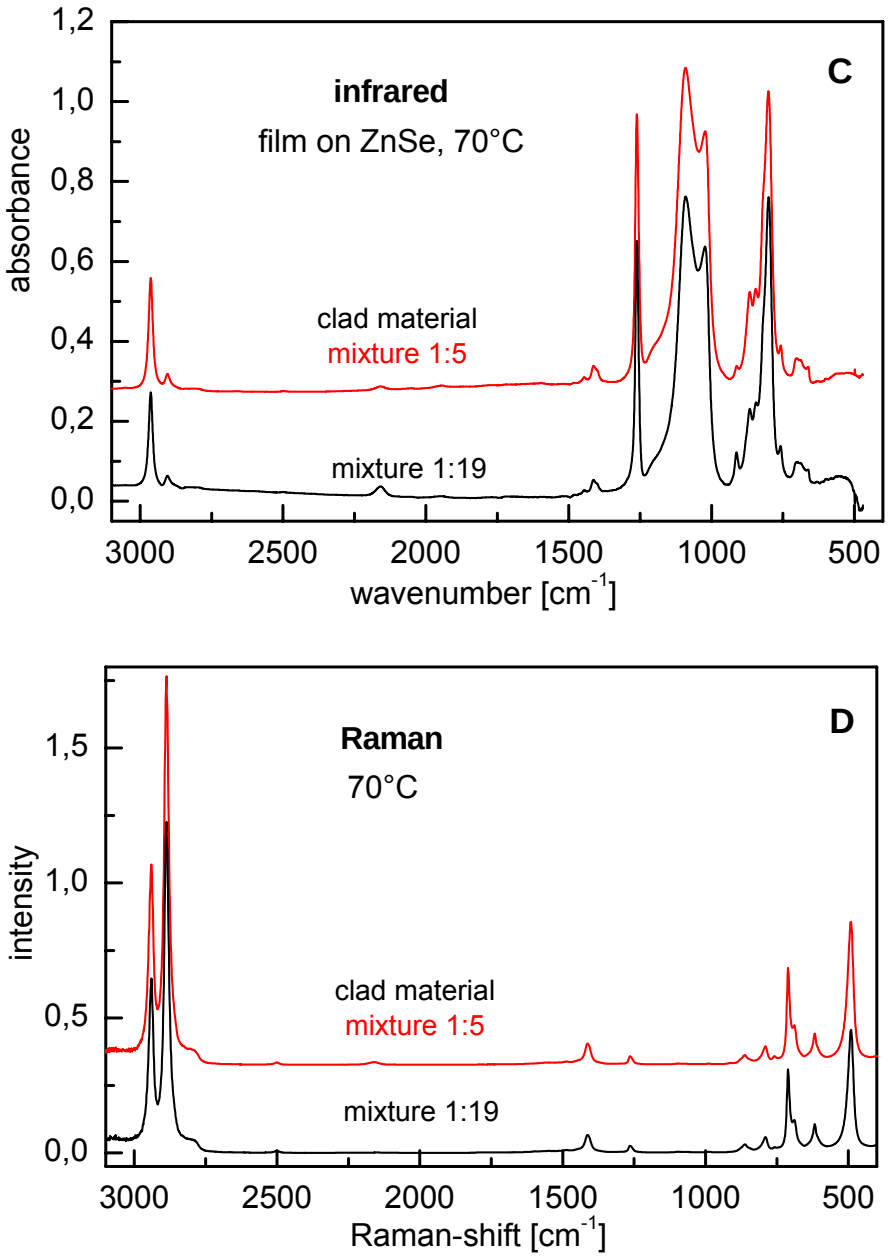


**Figure 4.4B** *FT-IR and FT-Raman spectra of PDMS crosslinked polymer (cladding)*

**Table 4.1** *The conversion (FT-IR and FT-Raman) of the reactive groups after curing at 70 $^{o}$C for 2 hrs for the PDMS networks*

| ***PDMS blending ratio (A:B)*** | ***Conversion Si-H (%)*** | ***Conversion Si-CH=CH$_2$ (%)*** |
|---|---|---|
| 19:1 | 79 | 72 |
| 5:1 | 87 | 78 |

With respect to 5: 1 blending ratio PDMS, it includes relatively more Si-H groups, whereas the conversion of the Si-H groups is higher than the conversion of Si-vinyl, it can be proposed to be a consequence of side reactions (post-cure) for which the following possibilities shown in equations 4.2 and 4.4. However, to 19: 1 blending PDMS, there are less Si-H groups reacted in post-cure stage and more is hydrosilylation crosslinking and thus the blending ratio is recommended for application of RT 601 cladding PDMS on waveguide fabrication for post-cure reaction can make PDMS network shrink and bring some by-products, e.g. bubbles.

Certainly the sensitivity for these Si-H side reactions is also strongly related with the presence of the platinum catalyst. They indicate that PDMS can potentially react with some polar components e.g. OH and carbonyl etc. on substrates through dehydration and hydrogen bonds (See Eq. 4.5 and 4.6) and enable PDMS bond with substrates under some specific conditions, which gives us hint that the PDMS might adhere to substrates through increasing the concentrations of Si-H groups and platinum catalyst for Pt catalyst can increase the velocity of post-cure reactions in some extents. It will be verified in the later parts.

$$\equiv Si - H + H_2O \xrightarrow[T^oC,\,t]{Pt\ catalyst} \equiv Si - OH + H_2 \uparrow \qquad (4.5)$$

$$\equiv Si - OH + OH - Substrate \xrightarrow{T^oC,\,t} \equiv Si - O - Substrate + H_2O \uparrow \text{ and}$$

$$\equiv Si - H + OH - Substrate \xrightarrow[T^oC,\,t]{Pt\ catalyst} \equiv Si - O - Substrate + H_2 \uparrow \qquad (4.6)$$

Additionally from spectrum of 5:1 blending cured PDMS it indicates that the conversion of Si-CH=CH$_2$ bonds can be increased by using an excess of Si-H bonds.

Furthermore, temperature influence on PDMS curing is also investigated with one 19:1 blending PDMS. The measured spectra in different curing conditions are

shown in Fig. 4.5.

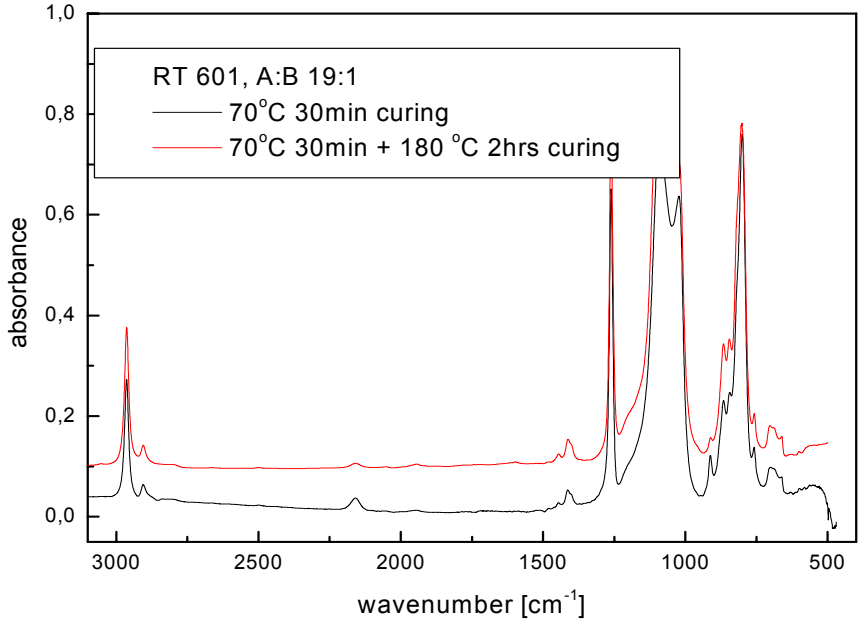


**Figure 4.5** *FT-IR spectra of PDMS cured in different temperatures*

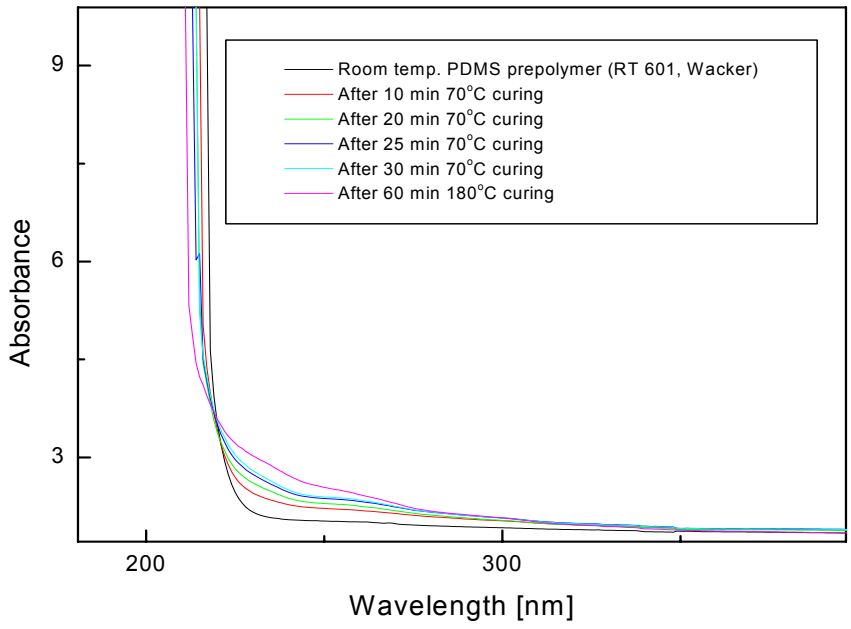


**Figure 4.6** *UV-Vis spectra of cured PDMS at different temperatures*

After further 180 °C for 2 hrs curing the conversion ratio of Si-H is obviously is

increased to be 87 % and the conversion of Si-vinyl to be 78 % from respective 99 % and 62 %. We thought the further high temperature treatment not only leads to hydrosilylation crosslinking but the Si-H react with water diffused into PDMS through post-cure reactions.

Beside IR and Raman spectroscopies one easy way is to use UV-VIS spectroscopy on monitoring PDMS curing state, since Si-CH=$CH_2$ bonds have strong absorption peak at 260 nm arising from electronic transitions.[75] After curing, the absorption peak at 260 nm will shrink with the elimination of vinyl groups in PDMS and shift to deep UV region, which is shown in Fig. 4.6.

### 4.2.3 Identification of Curing Conditions for PDMS Waveguides Fabrication

The critical issue in PDMS waveguides fabrication is that it must keep core PDMS strongly adhere to both cladding PDMS layers and the first cladding bond strongly with second cladding layer without any by-products as well as its good structure fidelity of cores with the respective grooves in the casting mould. Through analysis above, within post-cure reactions PDMS probably adhere to substrates with the increase of the concentrations of Si-H groups, but by-products from these reactions can cause waveguides shrink and lots of bubbles in the waveguides layer as well. Therefore, in PDMS waveguides fabrication PDMS post-cure reaction should be avoided.

In chapter 4.2.2, curing of RT 601 cladding PDMS has been studied with UV-VIS, IR and Raman spectra, and we found that 19:1 blending can make it have more hydrosilylation crosslinking and thus the blending ratio between base component and crosslinker is set to be 19: 1. To core PDMS (SLM 77522), due to its relatively shorter molecular chain and some specific structures applied for refractive index tuning we set it to be 9:1 after analysis of IR spectra of core PDMS with different mixing ratio like last chapter. Except identifying the appropriate blending ratios to achieve more hydrosilylation in PDMS curing, the curing time and temperature will be very important factors to determine the bonding quality between PDMS core and cladding etc. Through lots of pull-off measurements on PDMS waveguides layers (as to detailed measurement methods, please refer to chapter 4.2.4 B) and their cross-section observation with microscopy we found 70 °C for 30 ± 5 min curing is the optimum condition for core PDMS (SLM 77522) curing and first cladding PDMS layer curing. Under such conditions, core PDMS layer can strongly adhere to both cladding PDMS layers and first cladding bond strongly with second

cladding layer with good structure fidelity from the mould groove. In the following half part, with measured FTIR spectra of core PDMS we will in detailed explain and analyze the reason that we select such parameters.

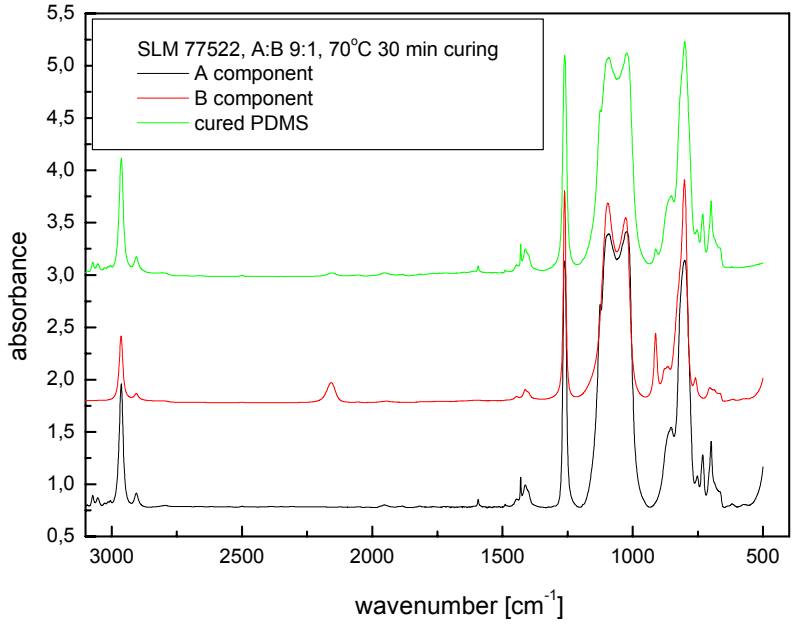


**Figure 4.7** *FT-IR spectra of core PDMS prepolymers and cured polymer*

From the spectra, we found a low conversation of Si-H bonds (65 %) and Si-vinyl bonds (45 %) in core PDMS based on the 70 °C for 30 min curing conditions but such conversation is proved enough to keep its robust mechanical properties and also to be demoulded from casting mould easily. Due to relatively low conversation ratio, lots of residual uncured reactive groups on the top surface of core PDMS layer might continue to react with respective groups, e.g. Si-vinyl vs SiH in cladding PDMS prepolymer through hydrosilylation reaction when they are poured onto the core PDMS in waveguide fabrication. The new hydrosilylation reaction between them will make them integrated together after some time thermal curing. Due to the incomplete curing, the network of core PDMS is not so dense that some parts with short molecule chain including reactive groups e.g. Si-H in cladding PDMS prepolymer may diffuse into core PDMS and react with Si-vinyl groups in core PDMS through hydrosilylation crosslinking, and finally make core and cladding bond strongly through chemical bonds. Whilst, after curing at 70 °C for 30 min of first cladding PDMS, its 99 % and 62 % conversation ratios of Si-H and Si-vinyl also can ensure it to form good bonding with second cladding PDMS layer for the

same mechanism. After pouring the 2nd cladding layer onto core and first cladding layer, it is suggested to make a little longer e.g. 1 - 2 hours curing to the whole realized waveguides, to keep further complete hydrosilylation reaction and reach better mechanical properties of the whole PDMS layer.

Then, as we found, the relatively larger mismatch between Si-H and Si-vinyl in 9: 1 core PDMS than 19: 1 cladding PDMS shown in Fig. 4.4 and beside the higher ratio of SiH bonds it can be explained as follows. Owing to the bulkiness of the phenyl group added to core PDMS for higher refractive index to keep optical waveguiding- and the increase in the number of branching (crosslink) points, the Si-vinyl and Si-H groups become more spatially hindered and have a fewer possibilities to react with each other. The higher conversions of the Si-H groups here should be a consequence of side reactions in post-cure stage. More Si-H side reactions will take place with an increasing amount of branching, because more end groups are present and capable of reacting with the Si-H groups.

### 4.2.4 Mechanical Characterization

### A. Relationship between molecular curing and mechanical properties of PDMS

Beside characterization with UV-VIS, IR and Raman spectrocopies, the state of curing of PDMS polymers can be directly reflected to their mechanical properties, e.g. tensile strength and elongation ratio at break, for they are strongly related with PDMS molecular chain length and crosslinking density. Thus PDMS polymers based on different curing conditions are prepared for the experimental verification.

Due to PDMS intrinsic low Young's modulus and high possion ratio, one mechanically optimized PMMA based casting mould (see Fig. 4.8) is designed based on FEM (Finite Element Method) mechanical simulation (Length: 110 mm; Width: 35 mm; Length of narrow part: 40 mm; Width of narrow part: 12 mm; Curve of neck place: 98 ± 1°) and fabricated with high precision diamond based micromilling machine. In order to avoid the shear strength during measurement, bottom and sidewall of mould are specially treated with UV exposure to achieve lower roughness (Ra< 20 nm). Furthermore during fabrication the PDMS layer in two wide side parts will be kept 1.5 - 2.5 mm thicker than the narrow part for they will sustain larger force when pressed by two clamps during pull test (See Fig. 4.8). The pull speed is 0.02 mm/ s. To every test item, 8 samples are prepared for measurement. The results are listed in Table 4.2.

**Table 4.2** *Mechanical properties of PDMS with different blending ratio and temperature treatments*

| | ***19:1 PDMS (70 °C 2 hrs)*** | ***5:1 PDMS (70 °C 2 hrs)*** | ***19:1 PDMS (70 °C 2 hrs + 180 °C 2hrs)*** |
|---|---|---|---|
| ***Tensile strength (MPa)*** | 1.42 ± 0.29 | 1.23 ± 0.34 | 1.49 ± 0.32 |
| ***Elongation at break (%)*** | 158 ± 7.92 | 112 ± 6.47 | 147 ± 0.29 |

**Fig. 4.8** *Casting mould for tensile strength measurement and set-up of pull off test*

In terms of aforementioned spectra analysis, it is clear that access of Si-H can obviously affect the PDMS robustness and elasticity properties due to post-cure reaction, for which causes much shorter molecular chain in PDMS network and relatively lower crosslinking density. The continuous high temperature curing indeed can increase the robustness of PDMS but the intrinsic good elasticity of PDMS elastomer is reduced, which is due to the post-cure reactions. Further hydrosilylation crosslinking can make Si-vinyl containing molecular chain react with Si-H containing molecular chain to form PDMS linear network structural unit and increase the crosslinking density and material intrinsic strength. However the post-cure reaction between Si-H with water etc. can decrease the materials elasticity due to its side reaction and low molecular chain properties.

## B. Limit strength in PDMS waveguides layer

In terms of PDMS waveguide fabrication method and curing conditions (70 °C for 30 min curing to core and first cladding, and 70 °C for 2 hrs curing to second cladding layer, i.e. the whole waveguides layer), the bulk PDMS waveguides layer including core and cladding is prepared. However, it is difficult to identify one appropriate method to correctly measure the limit strength of PDMS waveguides layer, for the actually used two-component PDMS prepolymer is well known for its reluctance to adhere to most of the substrates against curing. Then, as we knew cured PDMS can form good and strong bonding with glass sheets after $O_2$ plasma exposure and thermal treatment, so samples shown in Fig. 4.9 are prepared with two low roughness glass sheets (Middle part without metal chuck). They are separately put into $O_2$ plasma chamber for 0.5 - 1 min exposure and after that, pressing them together and drive the air bubbles out from their interfaces, then putting into 160 °C oven for 2 - 3 hrs thermal curing. After that the PDMS will strongly bond with the glass sheets. The glass sheets can be as a mechanical holder and inserted into two suitably sized metal chucks to be connected with force sensor (see Fig. 4.8). Then pull-off method can be used for identifying the limit strength of the bulk waveguides layer for intrinsic strength of glass is far stronger than PDMS applied here. After pull-off tests, it is found that strength limit of such PDMS waveguides layer is about 0.8 MPa and the damage of sample normally happens in the middle of waveguide cores for core PDMS applied here (SLM 77522) has relatively low tensile strength (0.57 MPa, and through adjusting the molecular chain length the intrinsic tensile strength can be improved to 2 MPa). Direct separations between core and both cladding layers, and first cladding and second cladding layer are not observed, which proves the core and cladding layers, first cladding and second cladding layers have been crosslinked each other to be one integration.

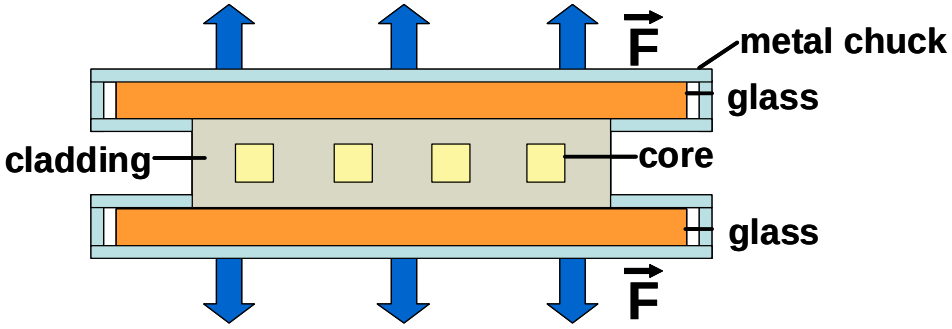


**Figure 4.9** *Cross-section of test specimens for determination of limit strength in PDMS*

*waveguides layer*

In conclusion, more hydrosilylation will improve PDMS crosslinking density and intrinsic mechanical properties which is also expected in PDMS waveguide fabrication, and then post-cure reactions also indicates that PDMS has potential to react with some polar components e.g. OH and carbonyl etc. on substrates through dehydration and hydrogen bonds under some specific conditions. After identifying the curing mechanism and various components functions in PDMS curing, based on different requests we have the capability to flexibly keep balance between main hydrosilylation and post-cure reactions through controlling curing temperature, the ratios of Si-H, Si-vinyl, inhibitor and platinum catalyst etc. Through adjusting curing parameters, the limit strength of PDMS waveguides layer can be directly up to the core material itself. Appropriate methods are identified to correctly measure the intrinsic tensile strength of PDMS polymer and the limit strength in PDMS waveguides layer.

## 4.3 Development of Surface-Adhesion-Promoter and Substrates Etching

The integration of multimode PDMS waveguides into conventional printed circuit boards is indeed very attractive because of low cost and easy manufacture. However, the actually used two-component PDMS prepolymer is well known for its reluctance to adhere to most of the substrates, especially to FR4 and copper, two most widely used substrates in general PCB manufactures. Unfortunately this property prevents the realization of self-packaged EOCB. Then according to our aforementioned research results about optical properties and loss contributors in PDMS and PDMS curing mechanism, in the chapter, from two aspects of surface adhesion promoter (SAP) development and substrates activation we will discuss how to realize the EOCB self-packaging under no extra influences on good optical, thermal, and mechanical properties of PDMS based EOCB.

In this chapter, FR4-boards, Kapton$^{TM}$ (polyimide, HN series from DuPont), copper coated FR4 boards and ED copper (Electrical Deposited as barrier layer for preventing outgas from some polymer based PCB substrates) are selected as PCB candidates' materials for research.

### 4.3.1 Basic Concept for Surface-Adhesion-Promoter Synthesis

To achieve good adhesion between PDMS and PCB substrates special Surface-Adhesion-Promoters (SAP) has to be developed. Though such RTV 2 PDMS is reluctant to adhere to most of the substrates, in terms of results in chapter 4.2 we found that PDMS has potential to react with some polar components e.g. OH and carbonyl etc. on substrates in post-cure stage through increasing the concentrations of platinum catalyst and Si-H groups. Additionally, by keeping balance between main hydrosilylation and post-cure reactions by controlling Pt concentrations, curing temperature and the ratios of Si-H and Si-vinyl etc., the PDMS polymers in terms of different requests, e.g. hardness, elasticity and bonding quality with substrates etc. may be synthesized respectively.

However, not like polymer substrates i.e. FR4 and Kapton, we can easily improve the concentrations of OH and carbonyl groups etc. on their surfaces through dry and wet etching which will be introduced in the following parts. With respect to PCB copper (Zinc covered copper, in chapter 4.3.3 it will be in detailed introduced) and ED copper, they are metals and obviously different with these polymer substrates, due to the highly ionic character of the metal-O bonds the covalent linkage to the siloxane group is chemically difficult. As we knew, Zinc has some catalyzing function to addition curing two components polysiloxane and Si-H bond can be added oxidatively to the zinc (0) atom and form colloid hydride Zinc containing ligand when the Si-H concentration and curing temperature are both high enough, and consequently they can be bonded together chemically. Thus it is necessary to protect the Zinc layer when it is micro-etched with $Na_2S_2O_8$ for organic contamination cleaning. To SAP applied for Zinc covered PCB copper, high concentration of Si-H groups and curing temperature are expected. However, with respect to ED copper, this method cannot be used any more for copper has no catalyzing function on such polysiloxane curing. In order to increase the possibility of reaction between SAP and copper substrates, the pure ‘post-cure’ reaction is expected for increasing the reaction possibility and thus the concentration of Si-viny groups in SAP should be as low as possible, additionally the surface of ED copper after organic contamination cleaning is proposed to be cleaned only with $N_2$ gas blowing not by drying in to avoid copper surface oxidized.

Based on such basic concepts to different boards, various surface adhesion promoters (SAP) containing different concentrations of Pt (0) catalyst ranging from 0.001 to 2 wt% and inhibitor ranging from 0.15 to 6 wt%, and different ratio between Si-H and Si-vinyl ranging from 1: 0 to 1: 100 are synthesized successfully in our Lab under that no any phase incompatibility and crystallizations exist, in addition the viscosity of SAP also can get controlled to be less 300 mPas for

meeting different fabrication requests, e.g. spray coating.

In the following parts, according to their different surface molecular structures, topography and distribution of polar components on substrates, their influences on bonding strength between SAP layer and PCB layer will be investigated in details after different etching treatments.

### 4.3.2 Identifications of Substrate Surface Molecular Structures and Appropriate Etching Methods

#### A. FR4

FR4 laminate is the usual base material from which plated-through-hole and multilayer printed circuit boards are constructed. It is the most versatile laminate and composite, this is a continuous glass woven fabric base impregnated with an epoxy resin binder whose synthesis is shown in Fig. 4.10.

It has extremely high mechanical strength, good dielectric loss properties, and good electric strength properties, both wet and dry. While the potential for environmental legislation is lessening in Europe (WEEE & RoHS),[76] primarily because Tetrabromo-Bisphenol A (TBBA) is not on the banned list, polybrominated aromatic compounds are still considered undesirable. The incineration of FR4 boards containing polybrominated aromatic compounds produces noxious Hydrogen Bromide (HBr) gas, which is corrosive.[77-79] Plastic materials that contain polybrominated biphenyls or polybrominated diphenyl ethers can be converted (oxidized) to dioxin or furan, respectively.80 Like introduced in chapter 3, they can not only harmer human but optical waveguides for they contain many vinyl groups which can absorb light near 850 nm wavelength.

While these specific flame retardants are not typically used in FR4 based PCBs, the perception is that PCBs will produce dioxin and furan derivatives upon thermal degradation. Toshiba has published data that indicates that no dioxins are formed upon incineration of PCBs using non-brominated resins with Phosphorous and inorganic based (some filler) chemistries.[81] “Green” labels are more common now in Europe. The European Community will most likely require OEMs to “take-back” electronic equipment. Future waste-management of PCBs containing halogens (and other environmentally unfriendly compounds) will most likely be costly. The main chemical families used for non-halogenated flame retardants are Phosphorous compounds, nitrogen compounds (including Polyamides and

Polyamines), oxy-acid sources like Boric, Sulfuric, and Phosphoric, and inorganic fillers and compounds containing Aluminum, Magnesium, or Red Phosphorous. Triazine derivatives are also effective flame-retardants.[80-82] In the thesis, FR4 boards (halogen free - non-brominated) were purchased from Isola GmbH, Düren, Germany.

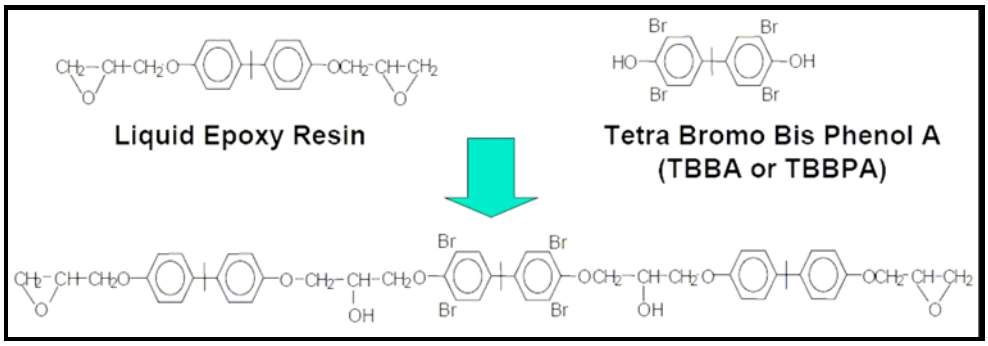


**Figure 4.10** *Basic synthesis concept of FR4*

Low pressure plasma treatment is probably the most versatile surface treatment technique to improve polar components concentrations on polymer substrates. It has become an important industrial process for modifying polymer surfaces which is usually confined to the top several hundred angstroms and does not affect the bulk properties. Oxygen and oxygen-containing plasmas are most commonly employed to modify polymer surfaces. In oxygen plasma, two processes occur simultaneously: etching of the polymer surface through the reactions of atomic oxygen with the surface hydrocarbon groups, giving volatile reaction products; and the formation of oxygen functional groups at the polymer surface through the reactions between the active species from the plasma and the surface atoms e.g. C-OH, C=O, O-C=O, C-O-O, and $CO_3$ etc. on the surface.[83-84] The balance of these two processes depends on the operation parameters of a given experiment. Actually many processes including $O_2$ plasma activation like introduced above followed by a surface graft polymerization. However, due to the restriction of high price of high vacuum plasma instruments, other appropriate low cost treatments are also necessary to be identified, e.g. wet chemical etching. Compared with plasma (vacuum) processes, these treatments are more preferred industrially. In the thesis, an alkaline oxidizing solution containing 1.25 - 2 mol/ l $KMnO_4$ and 1.25 - 2 mol/ l NaOH heating at 70 to 85 °C is applied as wet etchant to activate surfaces of polymer substrates, e.g. FR4 and Kapton (polyimide based) due to its potential on activating and modifying the carbon containing polymers surfaces physical and chemical characteristics. The function can be explained as follows

from equation 4.7 to 4.9.

Main reaction: $4MnO_4^- + 4OH^- + C < \text{fi } 4MnO_4^{2-} + CO_2 > +2H_2O$ (4.7)

In addition, the following reactions which happen on etchant itself should be avoided:

$$2MnO_4^- + 2OH^- \text{ f } 2MnO_4^{2-} + \frac{1}{2}O_2 > +H_2O \text{ on high PH value (4.8)}$$

$$MnO_4^- + H_2O \text{ f } MnO_2 + \frac{1}{2}O_2 > +2OH^- \text{ normal reaction (4.9)}$$

In the wet etching, concentrations of $MnO_4^-$ and $OH^-$, etching time and temperature will be the main deterministic factors. To ensure the etchant used repeatedly, first the concentrations of $KMO_4$ and NaOH cannot be so high, and additionally the electrochemical method combing with heating together also can be used to make them react in the reverse orient and avoid the deposition of $MnO_2$.

To study the influences of the effect of the $O_2$ plasma exposure and $KMnO_4$ etching on the final bonding strength, before and after the two etching on FR4-boards their surface molecular structure were both analyzed by FTIR/ ATR spectroscopy. Measured spectra are shown in Fig. 4.11. Among the most intense absorption peaks are those associated with -OH stretching (3700-3100 $cm^{-1}$), alkyl group (2960-2975 $cm^{-1}$), carbonyl group stretching (1720 $cm^{-1}$ out of phase and 1780 $cm^{-1}$ in phase), ester group (1739 and 1179 $cm^{-1}$), C=C in aromatic ring (1506 $cm^{-1}$), ether groups (1236, 1111, 1019 and 806 $cm^{-1}$), and epoxy group (914 $cm^{-1}$) etc.[85-87]

As seen in Fig. 4.11, in untreated FR4 substrate surfaces there also exist a few polar components, e.g. -OH and carbonyl, and lots of low surface energy non-polar alkyl groups. These few polar components on pure FR4-boards should enable reactions with –SiH containing groups in PDMS in terms of covalent and hydrogen bonds. However, the low surface energy of the alkyl groups on FR4-substrates can prevent the PDMS prepolymer wetting on FR4 substrate. To enhance the wettability of FR4-substrates and to improve the concentration of polar components, e.g. OH groups on it, low temperature $O_2$ plasma and $KMnO_4$ alkaline oxidizing solution (1.5 mol/ l $KMnO_4$ and 1.75 mol/ l NaOH) were applied. After 2 min and 10 min $O_2$ plasma exposure, and 30 min $KMnO_4$ wet etching on FR4 substrates, their spectra revealed that concentrations of various high surface energy polar oxygen complexes on the hydrophobic FR4 surface were increased, e.g. -OH and carbonyl groups etc. The concentrations change of oxygen complexes on FR4 surfaces is

due to the oxidation of FR4 surfaces by the two etching which is believed to proceed via a free radical, chain-reaction mechanism, whilst they also proves the two etching methods are both appropriate and effective on activating FR4 surfaces. The liquid solution etching by $KMnO_4$ can substitute to $O_2$ plasma for industrial application on FR4 etching and surface activation.

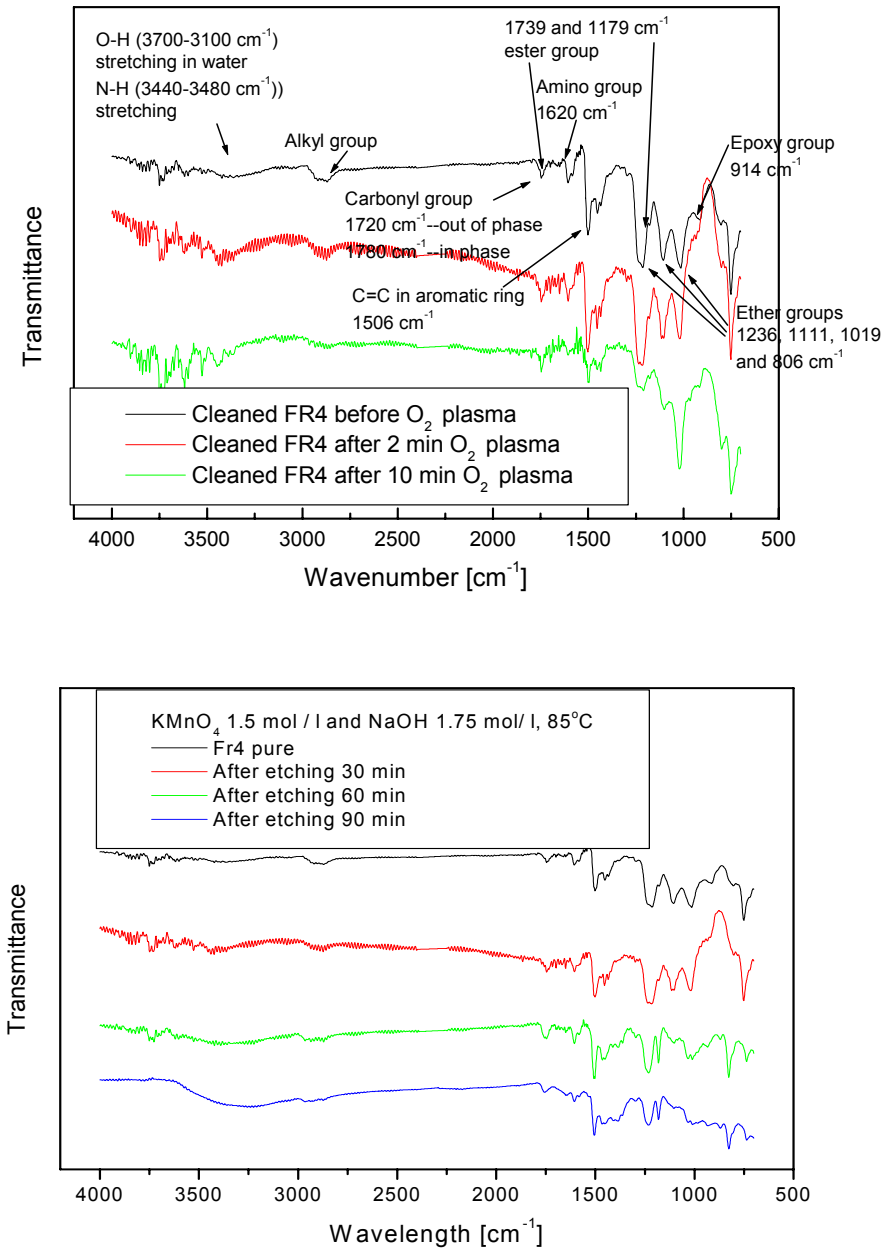


**Figure 4.11** *FTIR/ ATR spectra of FR4 surface before and after different etching*

## B. Kapton

The chemical structure of Kapton™ is shown in Fig. 4.12.[88] It has an amine $-NH_2$ group attached to the diphenyl ether group at various positions (ortho or meta). To Kapton, $O_2$ plasma exposure and $KMnO_4$ etching are also applied for etching only adjusting the $O_2$ gas from 20 % (to FR4) to 50 % and etching liquid solutions to be $KMnO_4$ of 1.75 mol/ l and NaOH of 2 mol/l due to Kapton's more robust molecular structures compared with FR4. To study the influence of the effect of the $O_2$ plasma exposure and $KMnO_4$ etching on the final bonding strength, the surface molecular structure of Kapton-board before and after the dry and wet etching were both analyzed by FTIR/ ATR spectroscopy and shown in Fig. 4.13.

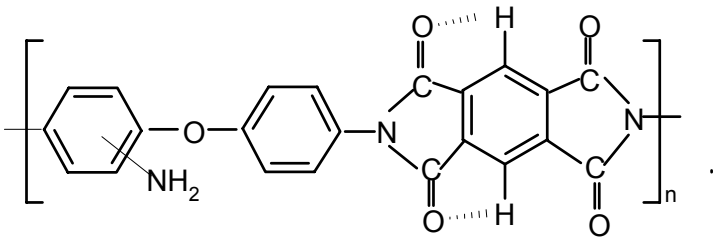


**Figure 4.12** *Chemical structure of Kapton™*

In terms of the spectra shown in Fig. 4.13, the characteristic absorption bands of kapton were assigned: 3700-3100 $cm^{-1}$ (-OH stretch), 3637, 3575 and 3479 $cm^{-1}$ ($-NH_2$ stretch), 3100-3000 $cm^{-1}$ (-CH in aromatic stretch), 1780 $cm^{-1}$ (cyclic imide -C=O in phase), 1712 $cm^{-1}$ (cyclic imide -C=O out of phase), 1609 $cm^{-1}$ ($-NH_2$ deformation bending), 1502 $cm^{-1}$ (aromatic ring C=C), 1370 $cm^{-1}$ (imide -CN), and 1236, 1111, 1013, 807 $cm^{-1}$ (ether).[89-91] As seen from the spectrum after 30s $O_2$ exposure, there are not largely different in the absorption of imide -CN group and aromatic C=C group. The absorption bands at 3700-3100 (-OH stretching peaks) $cm^{-1}$, 1780 $cm^{-1}$ (in phase C=O) and 1236, 1111, 1013, 807 $cm^{-1}$ (ether group) are slightly increased. Then the absorption bands at 3100-3000 $cm^{-1}$ (-CH in aromatic stretch), 3637, 3575 and 3479 $cm^{-1}$ ($-NH_2$ stretch), and 1712 $cm^{-1}$ (cyclic imide -C=O out of phase) is decreased, and the decrease of aromatic C-H band and $-NH_2$ are due to due to the loss of $-NH_2$ on the diphenyl ether group, and then the decrease of cyclic out of phase -C=O is possible due to the cleaning of organic contamination from the Kapton foil. To the spectrum of after 1 hour $KMnO_4$ etching, it has similar etching effects on Kapton surfaces but stronger, esp. OH groups, which got obviously increased.

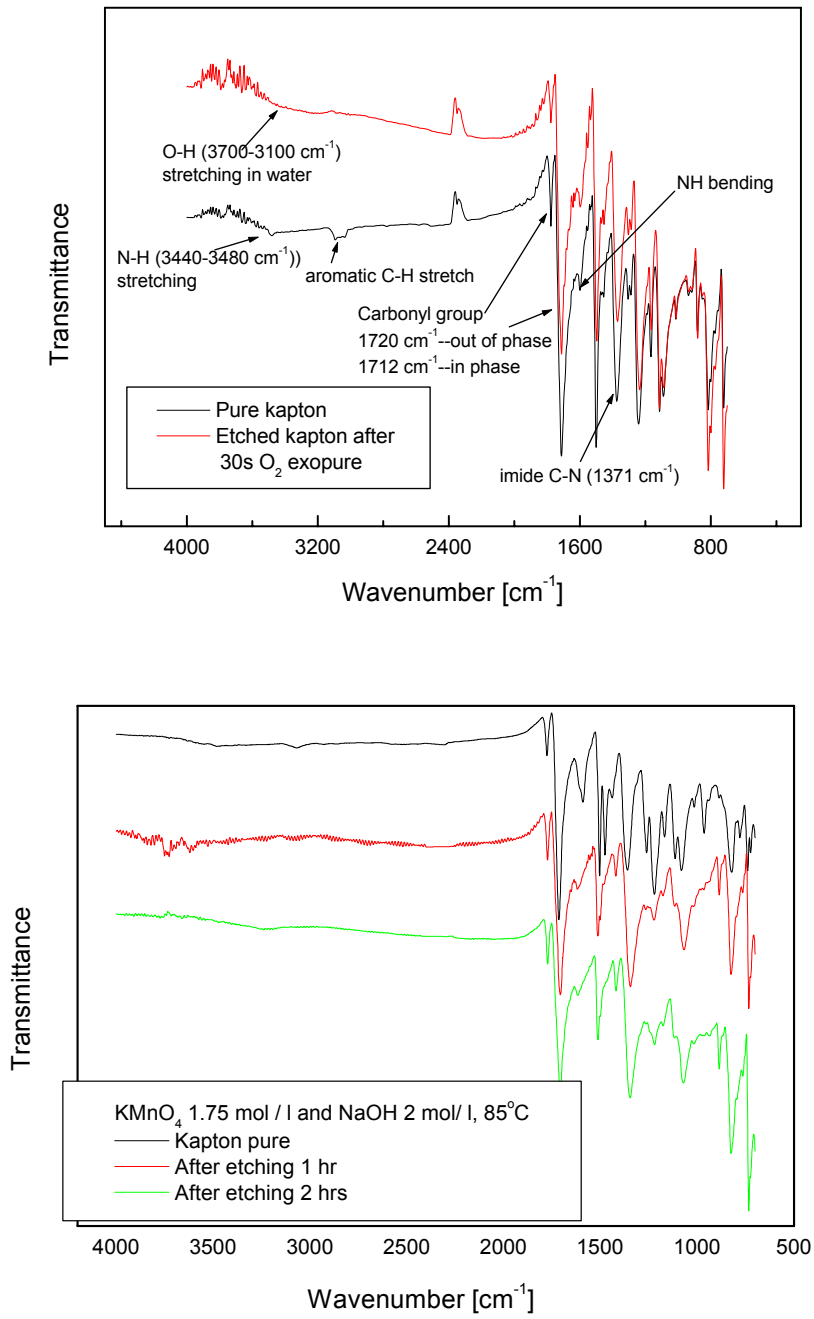


**Figure 4.13** *FTIR/ ATR spectra of Kapton surface before and after different etching*

Anyway, it indicates that reactive free radicals were formed by $O_2$ plasma exposure and $KMnO_4$ etching on the Kapton surface, colloid with the surface of Kapton, which introduced the oxygen-containing functional groups. In the process, free

radicals at the polymer surface were created by hydrogen abstraction in the $O_2$ plasma exposure and $KMnO_4$ etching. Then, these followed the formation of alkoxy radicals from the reaction of near-surface alkyl radicals with atomic oxygen, and they led to the formation of carbonyl groups etc. Also, like to FR4 substrates, the liquid etching solution including $KMnO_4$ can substitute to $O_2$ plasma for industrial application on Kapton etching and surface activation.

## C. Copper

In the thesis two kinds of copper based metals are applied in EOCB fabrication as EOCB carriers. One is the normal PCB copper (purchased from normal PCB vendors) and the other is ED copper (Electrical Deposited). Due to high purity and stable crystal structure of ED copper, here we will focus more on PCB copper and its surface elements distribution. In order to investigate the surface elements distribution of PCB copper, XPS/ AES (Auger electron spectrum) is applied for identification. In general, X-ray photoelectron spectroscopy (XPS) is widely used to obtain information about the elemental composition and the oxidation state of the elements being examined. Often the surface composition of a solid differs, at least to some degree, from the bulk composition. The high surface sensitivity provided by XPS is the greatest asset of the method in comparison with other surface analytical methods, esp. for metals. XPS/ AES spectrum and depth profile of pure PCB copper are illustrated in Fig. 4.14.

From the spectrum and depth-profile of copper surface, Zn and its oxidation state ZnO may be found everywhere and actually or say that a Zinc layer is on the copper layer. In order to investigate the real depth of this Zinc layer, $Ar^+$ sputtering is applied through driving out the surface element with high energy $Ar^+$ backscattering. It is found that about 20-50 nm Zinc layer (up to different PCB vendors) is on the copper layer which is treated as passivation layer for protecting copper from oxidization. Additionally about 10 % carbon is also found in the elements distribution, where small parts of them should be $CO_2$ absorption and most of them should be the organic contaminations.

To remove some organic contamination from surface under the precondition not damaging Zn passivation layer and obtain chemically pure and uniform surface for achieving better interface adhesion with PDMS, a kind of wet etching solvent called SENO 3207 ($Na_2S_2O_8$, Kepets) is used as the pre-treat etchant due to its relative low etching speed and the PH of etchant is adjusted at 4.0 - 4.3.

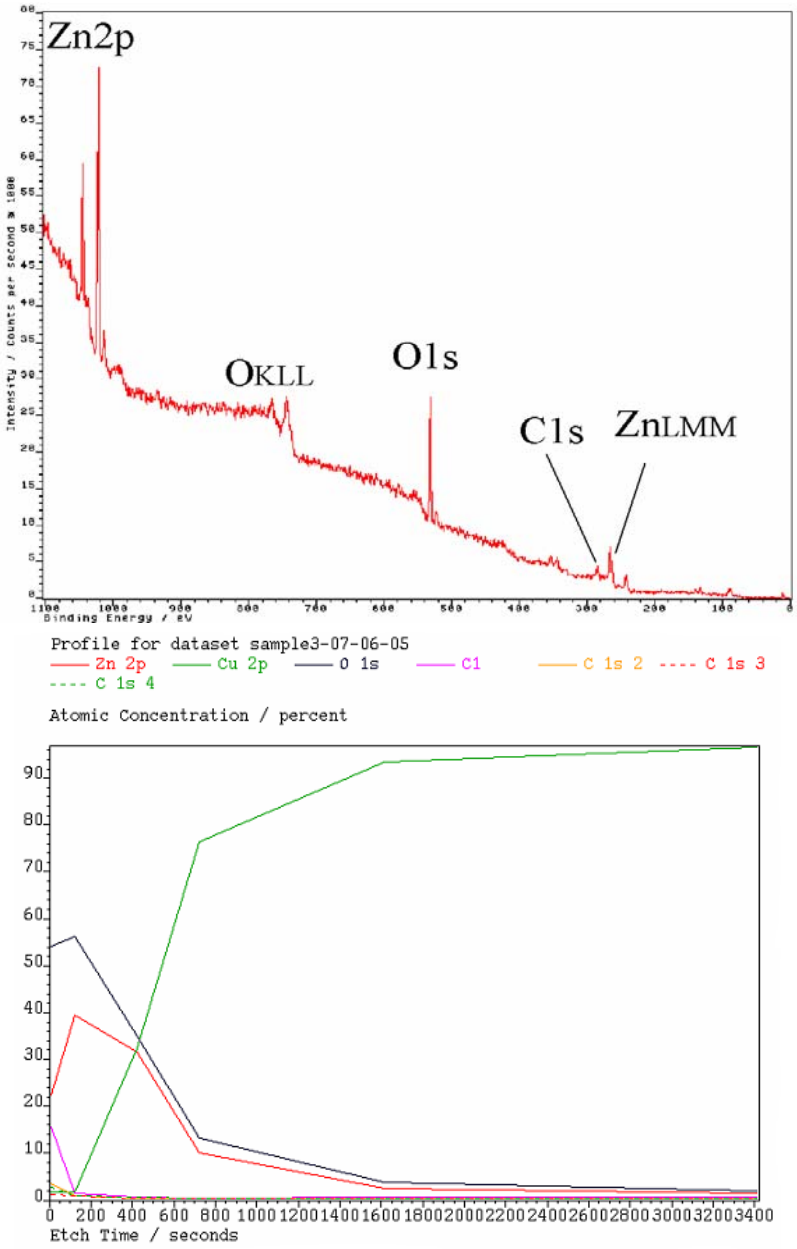


**Fig. 4.14** *XPS spectrum of PCB copper surface of Cu-Fr4 and depth-profile prior to etching*

The micro-etching mechanism can be illustrated below shown in equation 4.10:

$$Zn + S_2O_8^{2-} \text{ - fi } Zn^{2+} + 2SO_4^{2-},\ Zn + 2H^+ \text{ - fi } Zn^{2+} + H_2$$
$$ZnO + S_2O_8^{2-} + 2H^+ \text{ - fi } Zn^{2+} + 2SO_4^{2-} + H_2O \qquad (4.10)$$
$$3Cu + S_2O_8^{2-} + 2H^+ \text{ - fi } Cu^{2+} + 2Cu^+ + SO_4^{2-} + SO_3^{2-} + H_2O$$

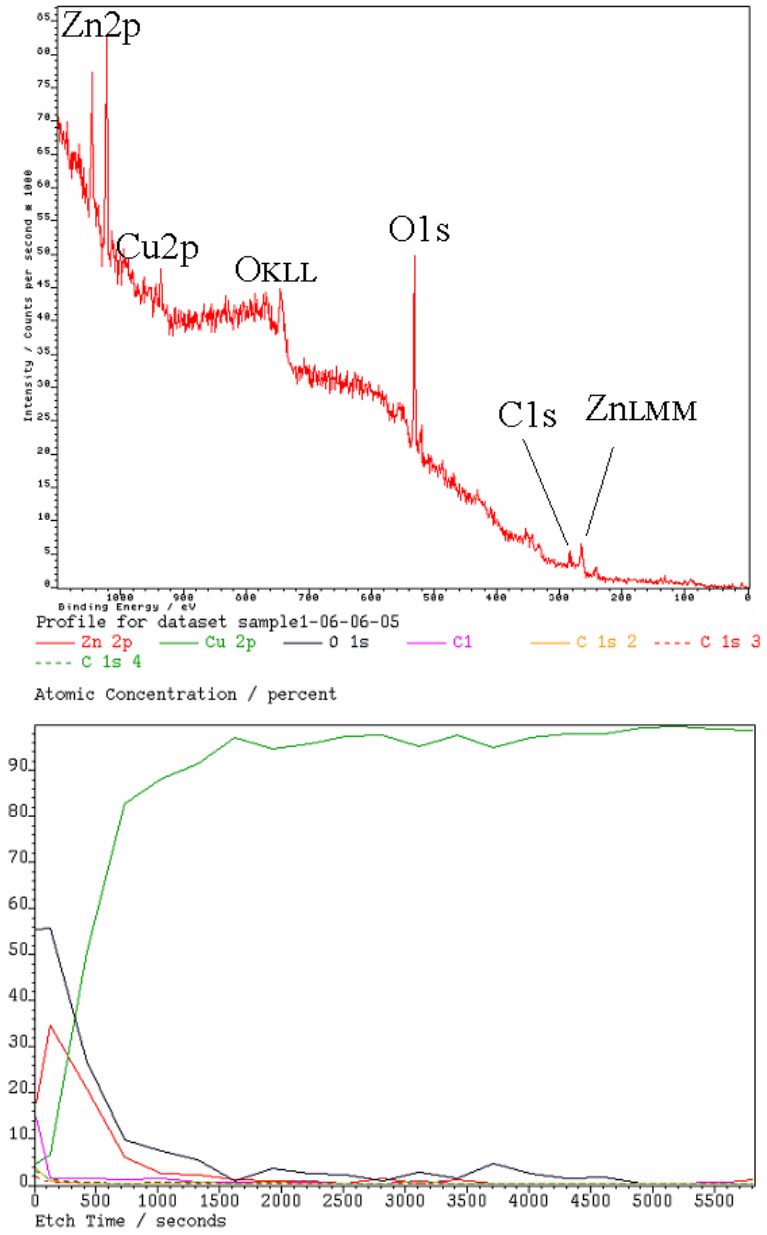


**Fig. 4.15** *XPS spectrum of copper surface of Cu-Fr4 and depth-profile after etching*

One PCB copper sample surface after 30s etching with 1 mol/ l $Na_2S_2O_8$ is checked with XPS spectrum and shown in Fig. 4.15. From their depth profiles, obviously Cu2p peak appears and C element amount is decreased due to removing of contamination compared with untreated PCB copper, but certainly the protection layer of Zinc also gets a little affected but not serious, which can get controlled through the etching time, concentration of etchant and PH value etc.

Additionally, for ED copper is also easily oxidized in air and we propose that it also should be etched with $Na_2S_2O_8$ before application in EOCB fabrication and the etching time is about 30 - 40 seconds.

### 4.3.3 Effect of Treatments on Surface Roughness

The positive effect of various etching treatments on the bonding strength between adhesives, like SAP and substrates is in part due to the chemical surface effects described in the previous chapter, but as well due to micro mechanical modifications of the surface. The reason is an increase of micro-roughness on the surface which leads to enlarged mechanical interlocking areas.

Good bonding occurs when the adhesive is able to penetrate into surface undulations like pores, holes and crevices. This causes the adhesive to mechanically lock into the surface of the substrate. For this to occur, the adhesive should be able to spread or wet the surface effectively and also possess the proper rheological properties to penetrate into the pores of the surface.

White-light-interferometer was used to quantify the roughness change on these PCB substrate-surfaces caused by various etching treatments. The arithmetic average surface roughness of substrates at different etching times is shown in Fig. 4.16. Obviously, there is no significant change on the FR4 and Kapton-substrate roughness after 10 min of $O_2$ plasma etching, and the copper-substrate roughness after 10 min wet etching as well.

Different with them, $KMnO_4$ containing oxidizer has a more profound influence on roughness. Roughness of FR4 and Kapton substrates both increase monotonously with an increase of oxidizing time due to large increase of oxygen contents at the surface, e.g. acid and ketone functions which are also shown in Fig. 4.11 and 4.13. However, to the two substrates the etching velocities are different due to their molecular structures. With respect to FR4 substrate, the increase of roughness is nearly linear with time for $KMnO_4$ oxidative treatment until a certain time, indicating a constant speed of roughness increase. The higher the speed of roughness increase, the smaller the treatment time at which the linear increase of roughness stops.

The constant speed of roughness formation indicated the existence of a pseudo-steady state for the polymer breaking down group scheme probably. Actually, the similar phenomena have also been reported recently, since the O/ C ratio is independent of the oxidation time.[61] In addition, to Kapton there even exists

one maximum with etching time increase, after which the roughness lowers slowly again. We think the pseudo-steady state and maximum lowers with increasing speed of roughness formation and hence may be also associated to diffusional limitations of the oxidizer, which influences the roughness evolution. The surfaces of FR4 and Kapton before and after $KMnO_4$ etching are observed with SEM as well, which is shown in Fig.4.17. Obviously, microcavities appear with longer etching times, which is possibly for the polar groups in these patches on substrates surfaces react with oxidizers and cause the formation of cavities. Pits of the order of a micro fraction appear in the surface of the polymer, as is well know from catalyses, pore diffusion is relatively slow and can easily limit reaction speeds. The polymer surface is constantly being etched away, and the cavities are formed by small differences in etching speed of the polymer. The pits are formed in the zones with highest oxidation speed. However, diffusion of the oxidizer through the pore is difficult and will limit the reaction speed as the pore depth increases. Due to these diffusional limitations, there exists one pseudo-steady state and the roughness will reach a maximum. This is probably the case for the fast $KMnO_4$ oxidation.

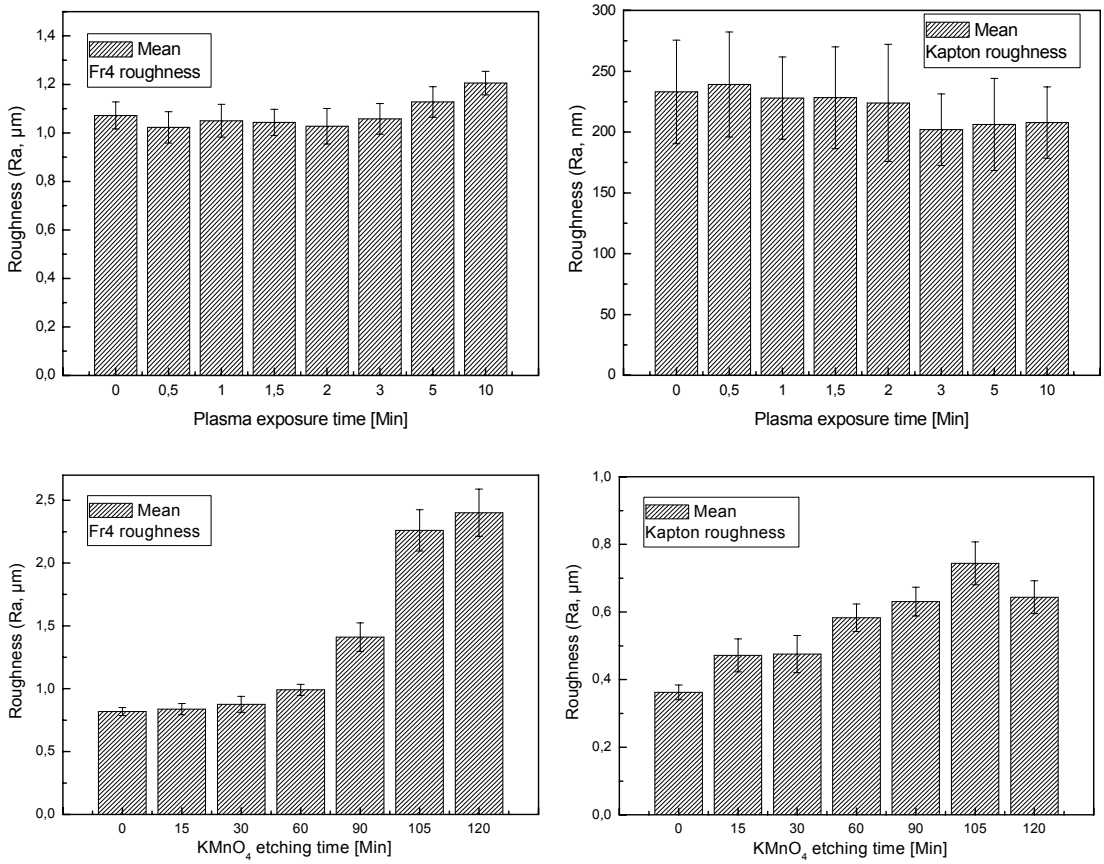

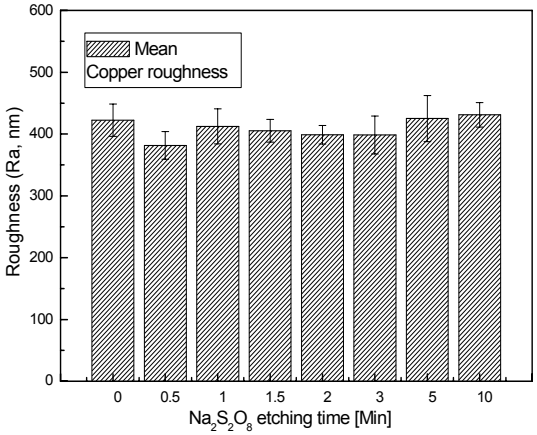


**Figure 4.16** *Effect of various etching on PCB substrates roughness*

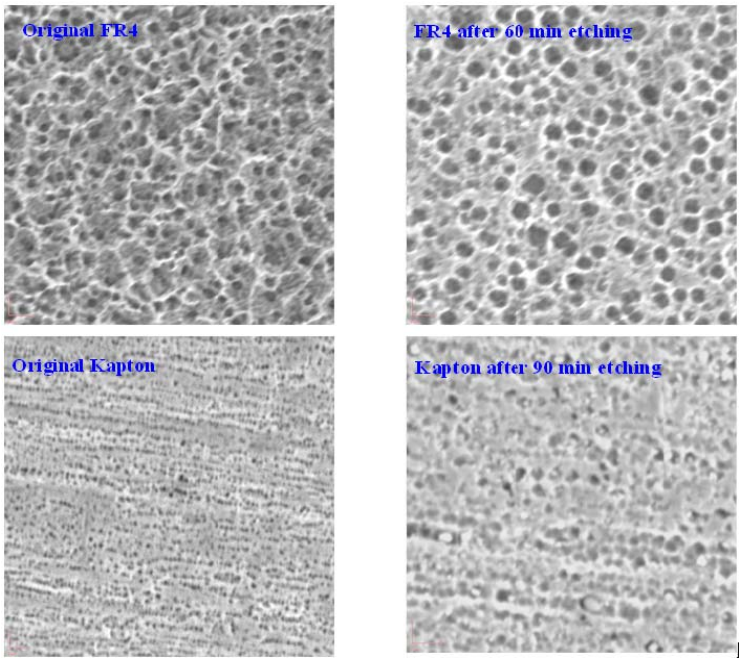


**Figure 4.17** *SEM images of FR4 and Kapton boards before and after etching*

### 4.3.4 Effect of Surface Etching on Surface Free Energies of Substrates

### A. Polymer substrates

FR4 and Kapton-surfaces are chemically activated by $O_2$ Plasma and $KMnO_4$ etching resulting in enhanced surface wettability and an improved concentration of

polar components. These can be determined by surface free energy analysis. A further advantage of the knowledge of the surface free energy is the following: when the values of surface free energies of solid polymers, esp. respective different components' surface energy value (e.g. polar or dispersive components), are close to those of liquid polymers e.g. SAP, the liquid polymers will have maximum wetting on the solid polymers. Therefore, it is necessary to identify the relationship between etching times and surface energy changes on FR4 and Kapton, so that we can modify the relevant SAP viscosity and surface energy to meet different substrates. Measurement of contact angles yield data, which reflect the thermodynamics of a liquid/ solid interaction. Surface free energy of a solid can be characterized and deduced from contact angle measurements between liquid and solid surfaces. The surface free energy of etched FR4 and Kapton-boards was determined using a sessile drop method combined with a microscope-camera system. Two different wetting liquids, i.e. distilled water and diiodomethane (nonpolar liquid), were selected for contact angle measurements.

The obtained contact angles are used to deduce the surface energy of the solid. In the estimation of surface free energy of polymer solids (FR4 and Kapton), the extended Fowke's equation and Young-Dupre's equation are widely used.[93] This approach divides the surface energy into two components, dispersive and polar, and uses a geometric mean approach to combine their contributions. The resulting equation (Eq. 4.11) when combined with Young's equation yields.

$$\gamma_l(1+\cos\theta) = 2\left(\sqrt{\gamma_{lp}\gamma_{sp}} + \sqrt{\gamma_{ld}\gamma_{sd}}\right),\ \gamma_l = \gamma_{ld} + \gamma_{lp} \text{ and } \gamma_s = \gamma_{sd} + \gamma_{sp} \quad (4.11)$$

where θ is the contact angle, $\gamma_l$ is liquid surface tension and $\gamma_s$ is the solid surface tension, or free energy. The addition of d and p in the superscripts refer to the dispersive (also called London dispersive) and polar components of each. The total free surface energy is merely the sum of its two component forces. The values of $\gamma_{lp}$ and $\gamma_{ld}$ are listed in Table 4.3. The values of $\gamma_{sp}$ and $\gamma_{ld}$ can be calculated based on the measured contact angles and the values of $\gamma_{lp}$ and $\gamma_{ld}$.

**Table 4.3** *London dispersive and polar components of wetting liquids surface tension, measured at 20 °C (mJ/ m²)*

| ***Wetting liquid*** | ***$\gamma_{lp}$ (mJ/ m²)*** | ***$\gamma_{ld}$ (mJ/ m²)*** | ***$\gamma_l$ (mJ/ m²)*** |
|---|---|---|---|
| $H_2O$ | 51.0 | 21.8 | 72.8 |
| $CH_2I_2$ | 50.42 | 0.38 | 50.8 |

Fig. 4.18 illustrates the results of surface free energies of the FR4 and Kapton-boards with respect to different etching times. The surface of untreated FR4 and Kapton-substrate is very hydrophobic, because of its low surface free energy, but hydrophilic after $O_2$ plasma exposure times of about 1 min (FR4), 30 seconds (Kapton), and wet etching of 15 min (FR4 and Kapton both).

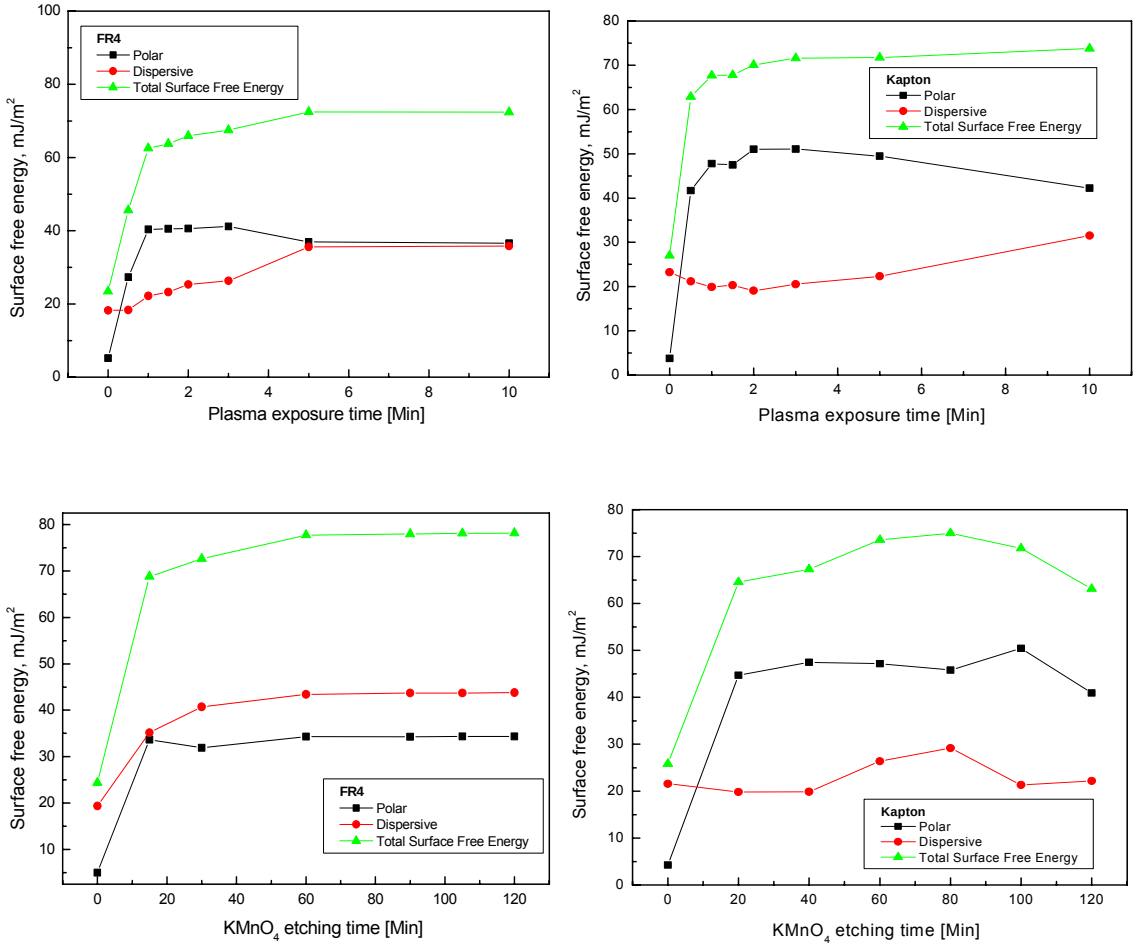


**Figure 4.18** *Surface free energies of the FR4 and Kapton-boards*

From Fig. 4.18 it is clear that polar components concentrations on FR4 and Kapton both have been largely increased after $O_2$ plasma exposure times of about 1 min and 0.5 min, and wet etching of about 15 min respectively, actually which are also related with and verified in their FT-IR spectra (Fig. 4.11 and 4.13). From those spectra, though the continuous etching can improve surface energy, whilst also damages the inner molecules of boards from surface due to the penetrated oxidizers (see Fig. 4.17), which will form one loose layer with poor mechanical

properties on bulk substrates and in reverse is disadvantageous to bond with SAP actually. The SAP will be able to form bonding with some polar components on FR4 and Kapton substrates through dehydration reaction and diploe-diploe interaction etc. and the maximum wetting happens on the condition that values of surface free energies of FR4 and Kapton, esp. respective different components' surface energy value (e.g. polar or dispersive components) are close to SAP respective components. So, Combing with analysis of Fig. 4.11 and 4.13, we can propose the boards' treatment conditions in general. With respect to $O_2$ plasma exposure, the etching times to FR4 and Kapton are proposed to be 1 - 2 min and with respect to $KMnO_4$ etching, the times are shifted to be 20 - 30 min.

## B. Copper substrates

Different with polymers substrates, beside the identification of various components surface energy and the relationship with etching times it is very important to identify one appropriate method to check the cleaning of organic contaminations on PCB copper substrate. So in the estimation of surface free energy of copper substrates, one Acid-Base (van Oss) equation and Young-Dupre's equation are used. It is proposed that the surface energy is composed of three components: lifshitz-van der Walls component $\gamma^{LW}$ including electromagnetic interaction, oscillation temporary dipoles interaction, and permanent and induced dipoles interaction; Lewis acid component ($\gamma^+$), which is related with the organic concentration on substrate; and Lewis base component ($\gamma^-$).[84] Their relationship is given by equation 4.12:

$$\gamma = \gamma^{LW} + 2(\gamma^+ \cdot \gamma^-)^{1/2} \qquad (4.12)$$

Due to three unknown parameters, three standard liquids (Water, ethylene glycol and diiodomethane) were used for measuring the surface energy and its three components of copper. Their surface energy and components are listed in Table 4.4.

**Table 4.4** *Surface tension of three liquids, measured at 20 °C (mJ/ $m^2$)*

| *Wetting liquid* | $\gamma^{LW}$ (mJ/ $m^2$) | $\gamma^+$ (mJ/ $m^2$) | $\gamma^-$ (mJ/ $m^2$) | $\gamma$ (mJ/ $m^2$) |
|---|---|---|---|---|
| $H_2O$ | 21.8 | 25.5 | 25.5 | 72.8 |
| $CH_2I_2$ | 50.8 | 0 | 0 | 50.8 |
| $HOC_2H_4OH$ | 29.0 | 1.9 | 47 | 47.9 |

Based on Young-Dupre's equation and Eqn. 4.12, the three components of surface energy of coppers are calculated after measuring the contact angles of the three liquids on them. The results are shown in Fig.4.19 where the green curve is related with general organic contamination for only it contains acid components. If magnifying, it can be observed to be decreased gradually with etching. Combing with the previous XPS analysis (see Fig. 4.14 and 4.15), we propose 1 - 2 min $Na_2S_2O_8$ etching time for copper treatment. Additionally the similar results are also achieved to ED copper.

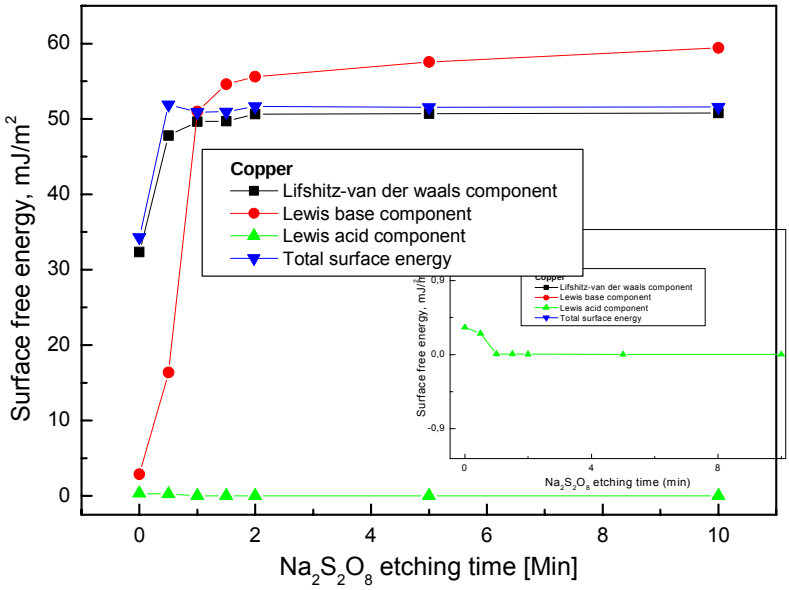


**Figure 4.19** *Surface free energies of PCB copper*

## 4.3.5 Influence from Hydrophobic Recovery on Treated PCB Substrates

The significant factor causing the limitation of the wettability and adhesion properties of substrates surfaces is the hydrophobic recovery of the etched surfaces. Hydrophobic recovery is a phenomenon that originates from the natural, thermodynamically driven tendency of surfaces to lower their free energy which can be shown by contact angle measurement on the treated polymer surfaces versus time. Actually, the decay of the contact angle change after treatments has been proposed to form by several mechanisms. They include recontamination by hydrocarbon onto polymer surfaces, the reorientation of polymer chains so as to bury covalently bonded polar functional groups, the migration of additives toward

the surface, and the diffusion of low molecular weight oxidized materials or called LMWOM towards the surface of the material. However the reorientation of polar moieties should be able to happen quickly, less than one minute, and thus the explanation is unlikely. The exudation of additives and LMWOM diffusion are both not likely either, because it is impossible that FR4 and Kapton substrates themselves contain lots of LMWOM like PDMS.[94-95]

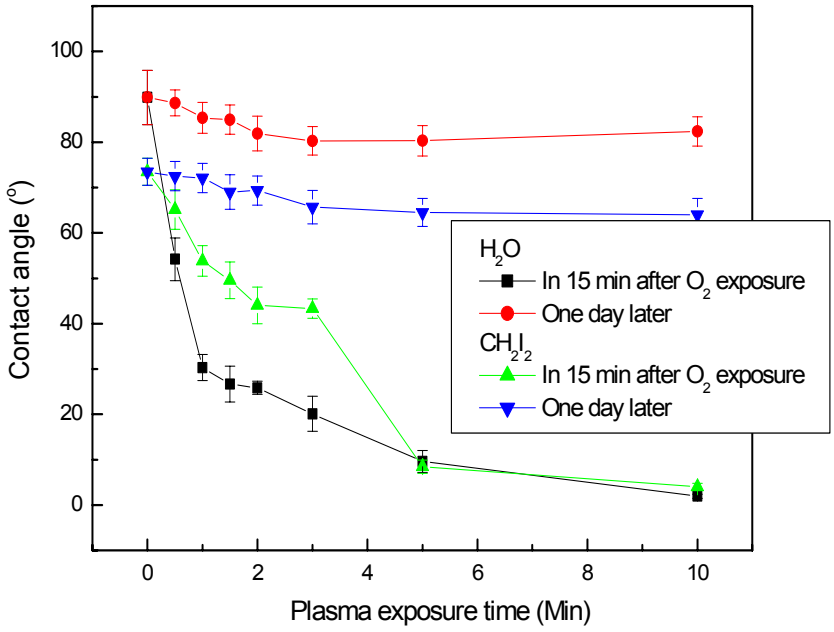


**Figure 4.20** *Decay of contact angle change with time*

Fig. 4.20 shows the experimental results of contact angles of distilled water and diiodomethane on $O_2$ plasma etched FR4-boards after 15 min and one day later. The contact angles of the liquids on the etched FR4-boards after one day show great increase. The wettability of surfaces nearly returns the original samples.

In addition, 180° peel-off tests (it will be in detailed introduced in the following chapter 4.4.2) were done with one-day stored $O_2$ plasma etched FR4-substrates again. It is found that the bonding strength between one specially synthesized SAP and FR4 is greatly decreased due to hydrophobic recovery. Also, it was verified that the 1.5 min $O_2$-plasma etched FR4-substrates can exhibit a good bonding together with the SAP within a period of 3 hours after the plasma treatment, which might be a reasonable time frame for a production line. Similar results are obtained for Kapton and coppers as well. In the table 4.5, the reasonable time frame is given according to different boards and etching methods.

**Table 4.5** *Valid time frame for boards use in EOCB fabrication after etching*

| | $O_2$ plasma | $KMnO_4$ | $Na_2S_2O_8$ |
|---|---|---|---|
| ***FR4*** | 3 hrs | One day | N.A |
| ***Kapton*** | 2 hrs | One day | N.A |
| ***PCB Copper*** | N.A | N.A | 1 hr |
| ***ED copper*** | N.A | N.A | 1 hr |

In the case, the main reason possibly causing the increase of contact angle of $H_2O$ and $CH_2I_2$ on the one-day stored FR4 and Kapton boards is the recontamination of the surface by hydrocarbon. On FR4 and Kapton boards they both consist of some low surface tension hydrocarbon structures besides hydrophilic polar groups e.g. cyclic imides and carbonyl etc. and they can have high affinity with hydrocarbon contamination after $O_2$ plasma treatment or $KMnO_4$ etching. The hydrocarbon with lower surface tension will enable the increase of contact angles and make surfaces hydrophobic.

## 4.4 Development of EOCB Fabrication based on SAPs and Compatible Etching Treatments

### 4.4.1 Basic Concept

In the aforementioned chapters we have identified the basic concept for SAPs synthesis and compatible methods for boards etching. Also, in chapter 3, we have identified that Pt catalyst, vinyl and phenyl groups can affect the PDMS optical properties and then actually in most SAPs products, they contain some Pt catalyst and vinyl containing polysiloxanes for obtaining better solvent compatibility and improving their dehydration reaction with substrates etc. In addition, in terms of EOCB fabrication steps, SAPs or SAPs mixed PDMS can possibly bond with casting mould after curing if treating them directly as cladding materials though we may tune its refractive index for waveguiding. Furthermore, the storage of treated substrates through aforementioned etching methods is also a critical issue restricting their practical application on EOCB production due to hydrophobic recovery. So, in order to avoid the influences from SAPs on optical waveguiding and extend the pot life of etched substrates, we propose to directly coat SAPs on

activated PCB substrates through spray coating or rolling etc. By controlling the curing temperature and time of SAP, the cured SAP layer can easily bond with cladding PDMS prepolymer through hydrosilylation reactions due to its consisting of Si-H groups and Pt catalyst as well. The cured SAP is as coating layer on PCB substrates and thus additionally, it also can prevent the activated surfaces from hydrophobic recovery to extend the pot life of these substrates longer.

Moreover, the bonding between SAPs and boards happens on the post-cure stage and there exist some by-products after the reactions, e.g. $H_2O$ and $H_2$ (see Eqn. 4.5 and 4.6). So the thickness of SAP layer is expected to be as thin as possible for elimination of bubbles on SAP layer. However, through experiments, we found that 70 µm thick cladding PDMS RT 601 (9: 1 mixture) can be cured at 90 °C after 20 min on copper substrate, but in 10 days it cannot be cured when the thickness is decreased to be 10 µm. Then, with the increase of Pt catalyst concentration it can be solved. The detailed experimental result is shown in Fig. 4.21. From the figure, with the increase of Pt catalyst concentration it is observed that the curing time is decreased dramatically. Further, the experiment is redone on non-polar components PDMS polymer surfaces and it is found the 10 µm thick PDMS layer can be easily cured in 60 min without any extra addition of Pt catalyst.

Compared with some similar results in other publications, we conclude that the possible reason is that the Pt catalyst in thin layer polysiloxanes is attached by polar components on substrates surfaces to the substrate surfaces and consequently affects hydrosilylation reaction. Specially, with respect to some FR4-like polymers which contain some electron donating compounds, for example organosulphur and amine etc. they can deactivate, inhibit and capture the Pt catalyst in PDMS and affect their curing.[71] Thus it is absolutely necessary to improve the concentration of Pt catalyst in various SAPs when they will be applied as thin layer coating onto such substrates. Moreover, compared with relatively thicker layer another advantageous of thin SAP layer- lower than 1 µm- is the limited mechanical influences on PCB substrates e.g. bow due to the Young's modulus and possion ratio mismatches.

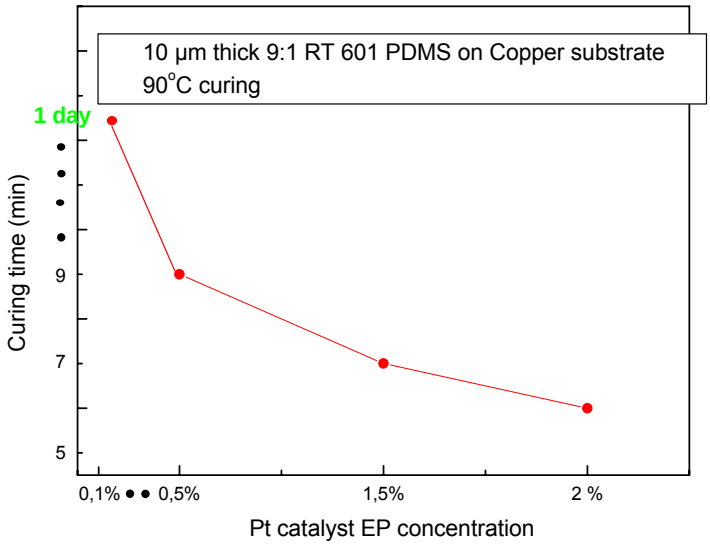


**Figure 4.21** *Thin layer PDMS curing on copper substrate*

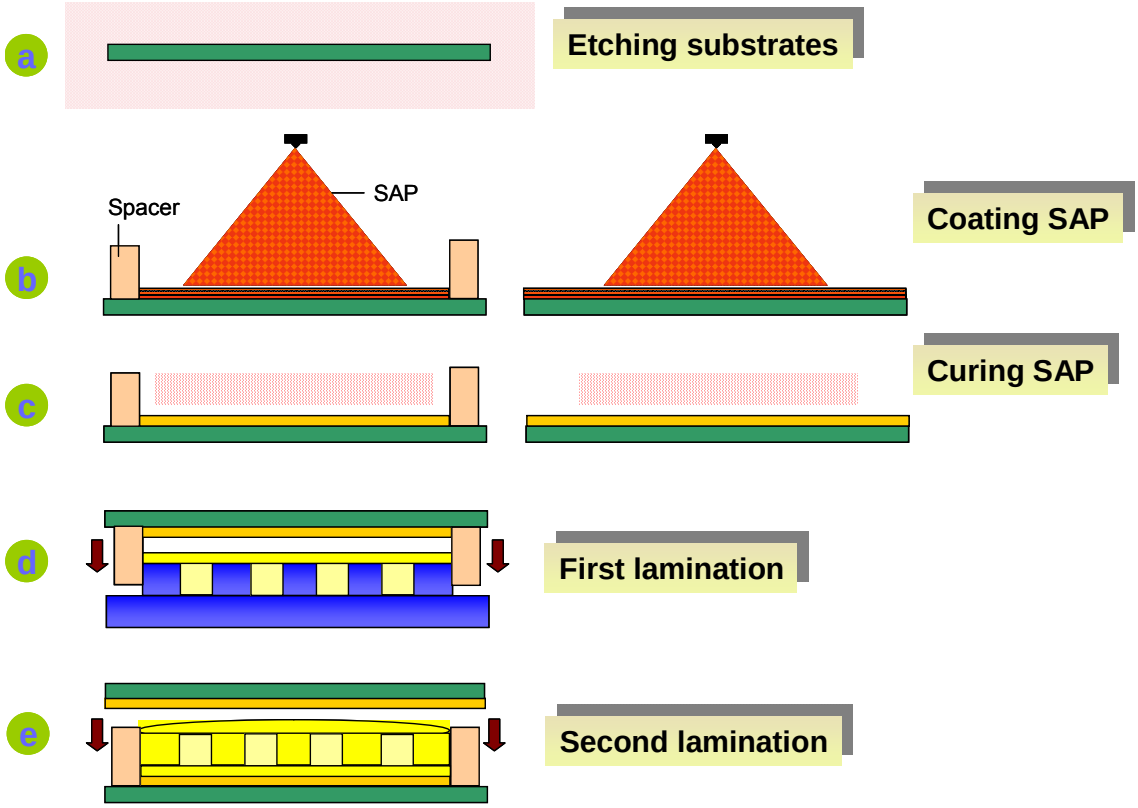


**Figure 4.22** *EOCB fabrication combining with SAP technique and boards etching*

The detailed procedure is shown in Fig. 4.22. Presently, this method is being transferred to worldwide first EOCB production project: Prospeos.

Based on the studied PDMS curing mechanism, the non-complete crosslinking of polysiloxanes can make them easily bonded with other polysiloxane prepolymer. So the determination of SAP layer curing condition is very vital to realize the EOCB packaging. The SAP layer cannot be fully cured; otherwise it will be difficultly bonded with liquid cladding PDMS against curing, but also not is too few, which will possibly lead to bubbles in cladding PDMS due to the post-cure reaction in cladding PDMS.

### 4.4.2 Determination of SAP Components and Etching Conditions

To examine the correlation between etching conditions on substrates and SAP components, one simple but effective 180°-peel-off test with pulling speed of 0.1 mm/ s was proposed and conducted (see Fig. 4.23) to identify the optimum treatments conditions to PCB substrates, SAP components and curing time etc.

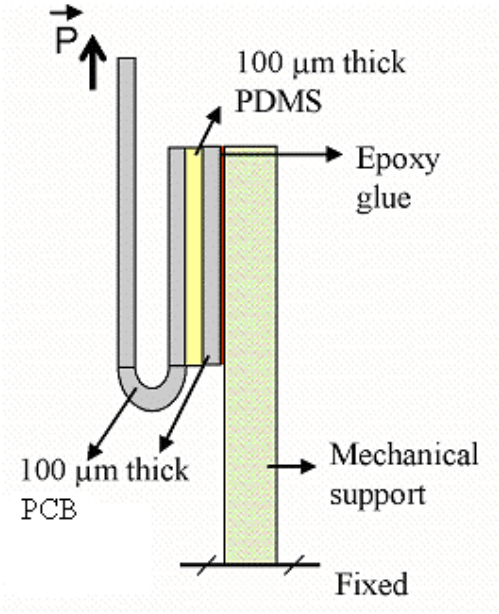


**Figure 4.23** *Schematic of 180°-peel-off test*

In the thesis, commercial RT 601 (Base component including Si-viny group called RT 601-A and crosslinker including Si-H groups called RT 601-B), H-Siloxane (methylhydrogen polysiloxane with trimethylsilyl endgroups), Catalyst EP (Pt

catalyst, 1, 1, 3, 3-Tetramethyl-1,3-Divinyldisiloxan- -platincomplex), PT 88 (Inhibitor) and AK 35 (Silicone oil for adjusting the viscosity of SAP) are selected as various basic constituents for SAPs synthesis and all of them are purchased from Wacker Chemie, Burghausen.

The prepared peel-off test sample is a Substrate-SAP-cladding PDMS-SAP-Substrate sandwich structure. Its dimensions are 10 cm in length, 1.5 cm in width, SAP layers thicknesss are both less than 1 µm and 100 µm in cladding PDMS thickness. As suggested by the name, peel-off test involves peeling of the top 100 µm thick FR4, Kapton, Zinc covered copper and ED copper coated PCB layers by fixing the bottom 100 µm thick layer on a stable mechanical support. From the measured peel force the peel energy ($G_{IC}$) can be determined through the following Eqn. 4.13 assuming that the extension of the peel strip is negligible.[96]

Peel-off energy equation:

$$G_{IC} = P(1 - \cos\theta)/b = 2P/b \text{ (for } \theta = 180^{o}) \quad (4.13)$$

where P is the peel force, θ is the peel angle and b is the width of the test sample. The average residual SAP area - i.e. unpeeled SAP area on both substrate boards - is observed as well. With respect to different boards, the different SAPs are synthesized and applied for sample preparation.

Through lots of experiments and combining with the proposed results in chapter 4.3, hereby we propose the treatments conditions, SAP components and SAP layers curing condition in EOCB fabrication as follows summarized in Table 4.6.

**Table 4.6** *Summarized optimum conditions for EOCB fabrication*

| | ***Components*** | ***Parameter of PCB materials*** | | | |
|---|---|---|---|---|---|
| | | ***FR4*** | ***Kapton*** | ***Zinc-Copper*** | ***ED copper*** |
| ***SAP components*** | RT601-A: B | 5: 1 | 5: 1 | 9: 1 | N.A |
| | Catalyst EP | 2 % | 2 % | 1 % | 2 % |
| | Inhibitor | 8 % | 8 % | 8 % | 7 % |
| | H-Siloxan | 10 % | 10 % | 15 % | 91 % |
| ***PCB-Material*** | Polymer-$O_2$ Plasma | 1.5 min | 1 min | N.A | N.A |

| | | | | | |
|---|---|---|---|---|---|
| ***Etching methods*** | Polymer-$KMnO_4$ | 30 min | 40 min | N.A | N.A |
| | $Na_2S_2O_8$ | N.A | N.A | 1.5 min | 1 min |
| ***SAP layer curing conditions (90 °C)*** | Polymer-$O_2$ Plasma | 8 - 10 min | 10 - 12 min | N.A | N.A |
| | Polymer-$KMnO_4$ | 10 min | 10 - 12 min | N.A | N.A |
| | $Na_2S_2O_8$ | N.A | N.A | 12 - 15 min | 15 - 20 min |

### 4.4.3 Characterization to Fabricated EOCB

### A. Mechanical characterization

The mechanical stability of fabricated EOCBs depends in a crucial way on the interfacial strength between the optical PDMS layer and the SAPs layer, and beteeen SAPs layer and PCB layer. If not strong enough, thermal stress resulting from coefficient of thermal expansion (CTE) and Young's modulus mismatch will cause delamination and therefore damage. The pull off test is widely used to test the adhesion of coatings to substrates. The prepared sandwich structure shown in Fig. 4.24 included a 200 µm thick cladding PDMS layer (19: 1) laminated between two SAPs coated various PCB carriers. The sample dimensions were 7 cm in length and 1.5 cm in width. After preparation, they were glued to an aluminium holder and measured under a pull speed of 0.02 mm/ s.

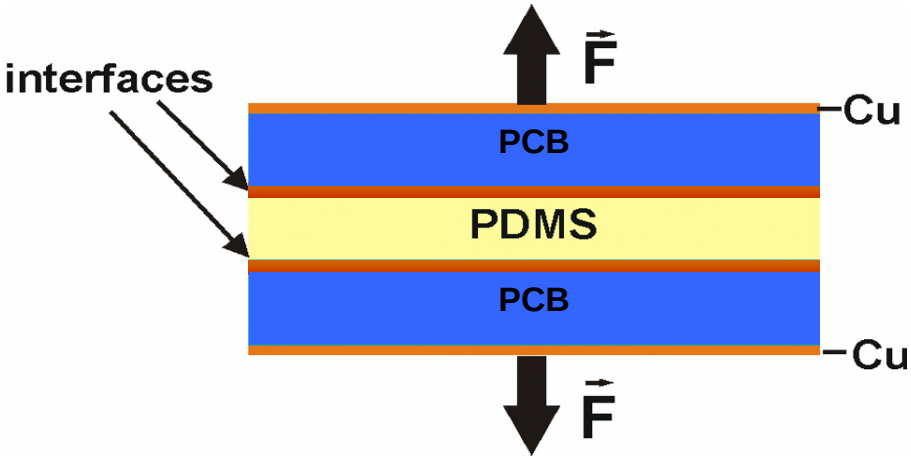


**Figure 4.24** *Schematic of pull-off test*

The measurement results are indicated in Table 4.7. The PRAA (largest percentage of residual adhesion area) of all samples is more than 95 %. By comparing these values with the measured stability limit of pure PDMS (1.35 ± 0.33 MPa) it is clear that the stability limit of the prepared samples is determined by the intrinsic material stability of cladding PDMS layer and not by the interface properties between SAPs and PCB substrates, and SAPs and cladding layer. A little larger pull strength of laminate than pure cladding PDMS is possible due to the following reasons. Some excess compounds in SAPs can indeed help cladding PDMS fully crosslinking e.g. Pt catalyst, in addition the thin layer crosslinking is also different with large dimension bulk sample and it can have more dense crosslinking in plane. The pull strength of copper and Kapton packaged samples is larger than FR4 packaged sample, because they have no inhibition effects on Pt catalyst and can ensure the cladding PDMS higher curing density.

**Table 4.7** *Test results of Pull strength of laminate*

| ***Test samples*** | ***Pull strength of laminate (MPa)*** | |
|---|---|---|
| | ***70 °C 2hrs curing*** | ***180 °C 2hrs curing*** |
| ***Cladding PDMS*** | 1.35 ± 0.33 | 1.42 ± 0.29 |
| ***PCB Copper/ PDMS*** | 1.38 ± 0.29 | 1.44 ± 0.32 |
| ***ED Copper/ PDMS*** | 1.41 ± 0.28 | 1.43 ± 0.21 |
| ***FR4/ PDMS ($O_2$ exposure)*** | 1.34 ± 0.32 | 1.36 ± 0.26 |
| ***Kapton/ PDMS ($O_2$ exposure)*** | 1.39 ± 0.23 | 1.44 ± 0.21 |
| ***FR4/ PDMS ($KMnO_4$ etching)*** | 1.35 ± 0.29 | 1.38 ± 0.26 |
| ***Kapton/ PDMS ($KMnO_4$ etching)*** | 1.42 ± 0.26 | 1.46 ± 0.27 |

## B. Ultrasonic scanning

Multilayer EOCB including not only more optical layers but also electronics layers will be the main development trend in the future. It means that general EOCB layer will be laminated with various PCB layers through high vacuum, high press and high temperature lamination process, e.g. to FR4: 0.3 bar, 180 °C for 2 hrs and 16 kp/ $cm^2$. In addition, in PCB manufacture, high vacuum plasma is also applied widely for via and PTH (Plated Through Hole) cleaning. So it will be very dangerous that air bubbles like defects exist in optical layer and interfaces which can cause EOCB delamination and even damage. During EOCB fabrication, some

air bubbles or water molecules in air can probably flow into PDMS and form defects. In the thesis, one non-destructive ultrasonic scanning method is proposed to identify the defects due to their different sonic transimission velocity in air, PDMS and PCB substrates. Through selecting appropriate scanning frequencies, it cannot only identify the sizes of defects but position them in EOCB by amplitude and depth analyses. With the help of the intensity and the distance traveled by the reflected waves, two kinds of reports namely, amplitude and depth analyses can be produced. The amplitude report shows the intensity of the reflected waves where as the report for depth shows the distance (depth) through which the waves are penetrated.

The ultrasonic device is provided with a transmitter and a receiver. A uniform beam of ultrasonic waves are cast on to the sample from one side. The waves penetrate through the board if there are no flaws or errors. On the other hand, if there are any flaws at some locations, the waves at those particular locations would reflect back.[97]

These reflected waves will be received by the receiver. Using the time taken for the to and fro traveling of the waves and the velocity of the ultrasonic waves, the distance could be calculated. The intensity of the reflected waves could also be known, which is, in fact, inversely proportional to the distance traveled.

The ultrasonic scanning report may have different colors which vary from red to violet. Different colors in the report indicate different amplitude/ depth at respective locations of the board. The reports are provided with a scale of colors (VIBGYOR) with the help of which the amplitude/ depth at particular locations could be studied. The scale provided in the amplitude report shows the intensity of the waves received by the receiver in terms of percentage. For instance, 100 % in the report implies that the waves are reflected from the outer surface of the board without penetrating into it.

As the waves penetrate deeper in to the board, the intensity will be gradually decreased. The scale provided in the depth report shows how deep the waves are penetrated into the board in terms of millimeters (in this EOCB case). To put it in another way, the length of the scale is nothing but the thickness of the board. The color with the minimum value indicates that the waves are reflected from the top surface of the board without penetrating into it. Whereas the color with the maximum indicates that the waves are completely penetrated to the other end of the board and reflected back.

In order to verify the validity of this method, one preliminary test to EOCB (Copper coated FR4-PDMS-Copper coated FR4) with ultrasonic scanning analysis has been performed and shown in the figures below.

Fig. 4.25 is the amplitude report of the sample. As the main focus of this thesis is on the optical layer of EOCB, it is better to observe the amplitude at the interfaces of the optical layer with the layers above and below it. As the velocity of the ultrasonic waves and the distance (depth) of the interfaces are known, the amplitude at the interfaces could be observed by calculating the time at which the ultrasonic waves cross the interfaces approximately.

It could be noticed from the figure that there are three samples of EOCB in this case. The part of the board outside the three samples is the excess board considered for marginal purposes. The interpretation of this part could be neglected. The focus is only on the EOCB samples. The PDMS regions in the figure are in blue color which indicates that the intensity of the ultrasonic waves is about 70 % to 80 %. The PDMS regions are almost uniform (with the same color), which means that there are no air bubbles in that region. The yellowish and aqua regions where the intensity of the ultrasonic waves is about 30 % to 50 % could be air bubbles in this case. The air bubbles inside the sample are dangerous and could lead to unexpected consequences. Therefore, it is always important to avoid air bubbles between the layers. To 3$^{rd}$ EOCB sample in Fig. 4.25, along with the bottom half margin the color shows that there are possible air bubbles. In the following, the assumption is also verified through cutting the sample and observing the cross-section with microscope.

Additionally, Fig. 4.26 shows the depth report for the sample. From the scale below the figure it can be understood that the ultrasonic waves have penetrated more through the green regions. The distance/depth traveled by the waves in the PDMS region is less due to relatively larger sonic impedance in PDMS.

Anyway, in analyzing the depth report, it is important to know that the sample has layers of different materials and the ultrasonic waves travel with different velocities through the materials with different properties. Because of this, the point or the layer from which the waves are being reflected could not be properly studied. Moreover, this analysis could lead to fallacious interpretations and assumptions due to its less penetration in PDMS area. Hence, depth analysis is not recommended as main analysis method on EOCB defect detect.

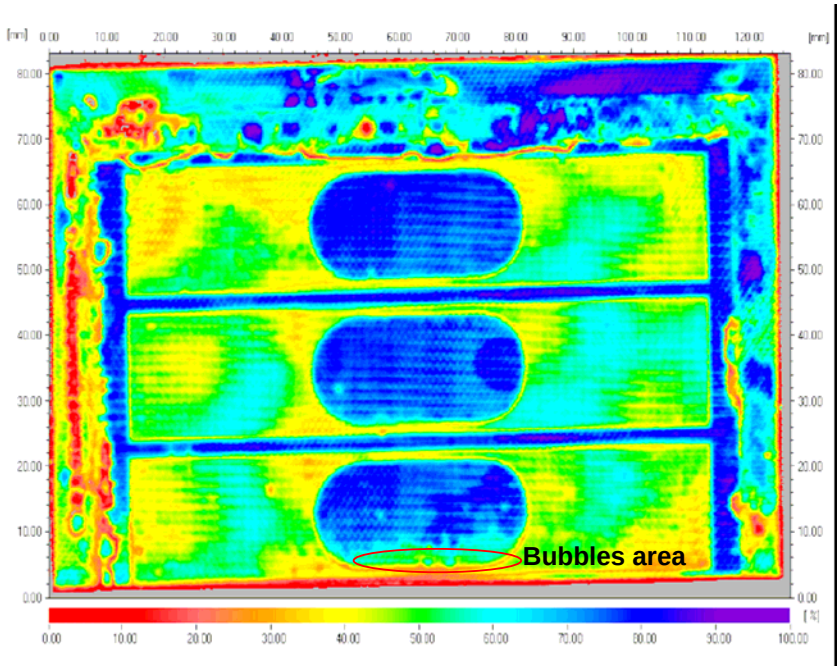


**Figure 4.25** *Ultrasonic Scanning report – Amplitude Analysis*

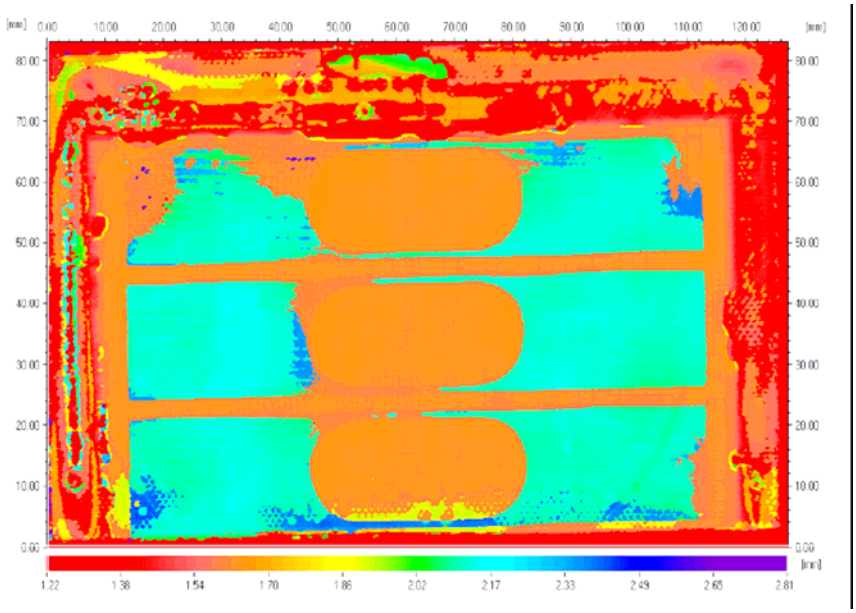

**Figure 4.26** *Ultrasonic Scanning report – Depth Analysis*

## C. Optical characterization

Optical waveguide transmission loss and mechanical stability are the two basic issues in EOCB specifications.

Here, the optical transmission loss of fabricated EOCBs has been measured at the standard wavelength for optical interconnects at 850 nm at different annealing conditions. Laser light was launched into the waveguides by a 50 µm GI fibre and detected by a 200 µm SI fibre. A transmission loss value of 0.035 dB/ cm was obtained which is almost that of a sample prepared without FR4 carriers (Fig.4.27, left column). After the measurement the sample was annealed at 180 °C for 2 hours which corresponds to the time and temperature conditions at multilayer PCB board lamination. The transmission loss shows a slight increase for the self-packaged EOCB to 0.04 dB/ cm and a decrease to 0.03 dB/ cm in case of the pure PDMS waveguide samples. This procedure is repeated at 260 °C for 1 min which represents the soldering condition.

As seen in Fig. 4.27, the waveguide loss of FR4 packaged EOCBs gets slightly increased compared with pure PDMS waveguide samples, but is still under 0.06 dB/ cm - even after annealing up to 260 °C/ 1min. Similar results are also obtained to Kapton, PCB copper and ED copper packaged EOCBs.

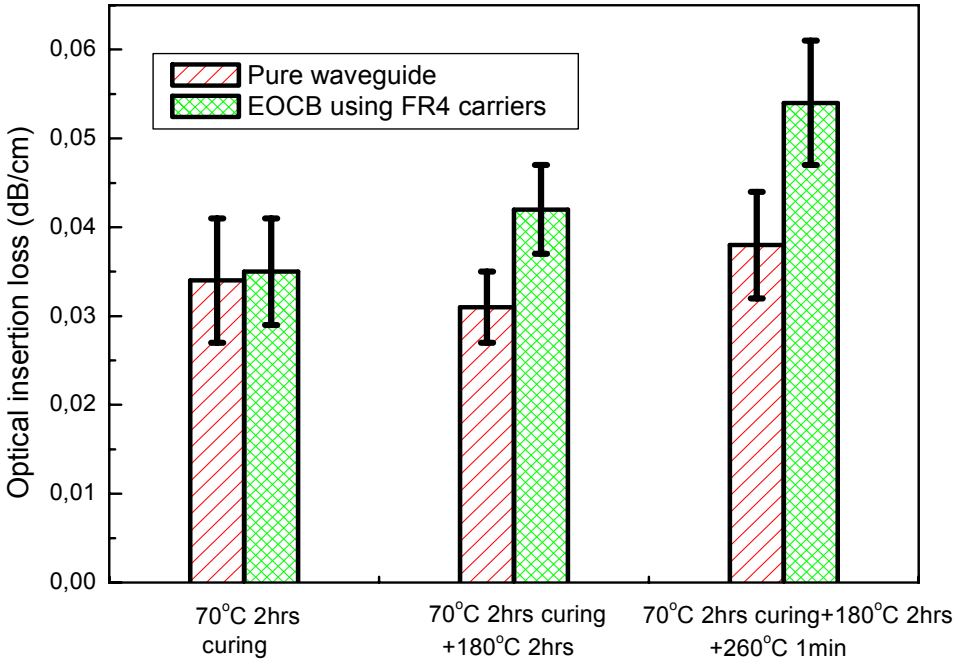


**Figure 4.27** *Thermal stability of EOCB optical transmission loss*

In conclusion, fabricated EOCBs show sufficiently low optical transmission loss as

well as thermal stability to overcome standard PCB manufacturing conditions.

## 4.5 Environmental Stability of Realized EOCB

Electrical-optical circuit boards are investigated worldwide to overcome the problems arising from high speed signal transmission in high power computing systems. In previous chapters, most of the research work reported is focused on materials, fabrication technologies and identification to characterization methods etc. However, for an industrial implementation of EOCBs, a reliable production technology as well as a corresponding quality management must be developed. In the part the environmental stability of the optical and mechanical properties of fabricated PDMS based EOCBs based on SAP coating and board etching technologies is presented. The test methods are based on the standards for optical components in telecommunications (Telcordia) and general PCB tests (IPC and IEC).

### 4.5.1 Environmental Accelerated Testing Design

The concept of accelerated testing is to compress time and accelerate the failure mechanisms in a reasonable test period so that product reliability can be assessed. The only way to accelerate time is to stress potential failure modes. These include electrical and mechanical failures. Figure 4.28 shows the basic concept of stress testing. Failure occurs when the stress exceeds the product's strength.

In a product's population, the strength is generally distributed and usually degrades over time. Applying stress simply simulates aging. Increasing stress increases the unreliability (shown in Figure 4.28 as the overlap area between the strength and stress distributions) and improves the chances for failure occurring in a shorter period of time.

This also means that a smaller sample population of devices can be tested with an increased probability of finding failure. Stress testing amplifies unreliability so failure can be detected sooner. Accelerated life tests are also used extensively to help make predictions. Predictions can be limited when testing small sample sizes. Predictions can be erroneously based on the assumption that life-test results are representative of the entire population. Therefore, it can be difficult to design an efficient experiment that yields enough failures so that the measures of uncertainty in the predictions are not too large. Stresses can also be unrealistic. Fortunately, it

is generally rare for an increased stress to cause anomalous failures, especially if common sense guidelines are observed.[98]

Anomalous testing failures can occur when testing pushes the limits of the material out of the region of the intended design capability. The natural question to ask is: What should the guidelines be for designing proper accelerated tests and evaluating failures? The answer is: Judgment is required by management and engineering staff to make the correct decisions in this regard. To aid such decisions, the following guidelines are provided:

1). Always refer to the literature to see what has been done in the area of accelerated testing.

2). Avoid accelerated stresses that cause “nonlinearities,” unless such stresses are plausible in product-use conditions. Anomalous failures occur when accelerated stress causes “nonlinearities” in the product. For example, material changing phases from solid to liquid, as in a chemical “nonlinear” phase transition (e.g., solder melting, intermetallic changes, etc.); an electric spark in a material is an electrical nonlinearity; material breakage compared to material flexing is a mechanical nonlinearity.

3). Tests can be designed in two ways: by avoiding high stresses or by allowing them, which may or may not cause nonlinear stresses. In the latter test design, a concurrent engineering design team reviews all failures and decides if a failure is anomalous or not. Then a decision is made whether or not to fix the problem. Conservative decisions may result in fixing some anomalous failures. This is not a concern when time and money permit fixing all problems. The problem occurs when normal failures are labeled incorrectly as anomalous and no corrective action is taken.

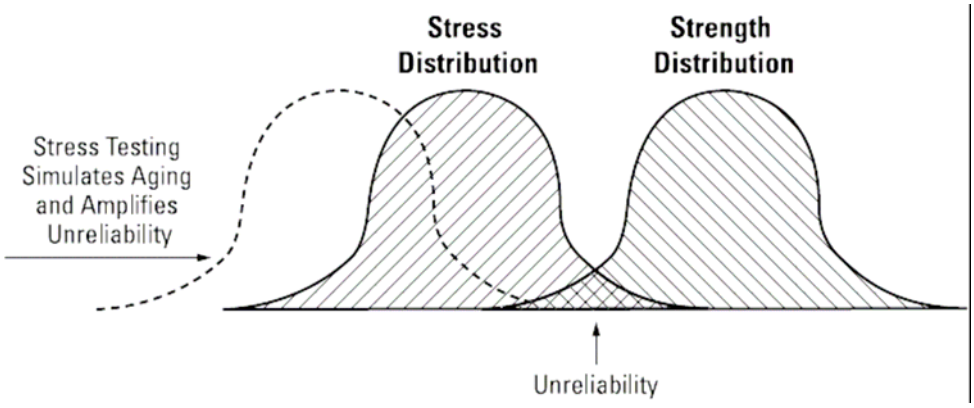


**Figure 4.28** *Principal of accelerated test*

However, presently there are no any existing environmental stability standard test procedures for EOCBs, in the thesis for the first time we define the test procedures by combining general PCB test methods (e.g. IPC-TM-650 and IEC 99) together with standard test methods for optical components in telecommunications (e.g. Telcordia standards GR-1220 and GR-1209) as test methods for verification of EOCBs environmental stability. From these methods and standards, based on our experiences and knowledge to EOCB materials and products, and similar literatures on PDMS based products environmental tests the following test items significantly related with environmental stability have been identified:

A. Tests against reliability during fabrication

1) Lamination conditions: 180 °C for 2 hrs., 16 kp/ $cm^2$ (To FR4);

2) Solder floating: 3 times 10 s solder floating at 260 °C.

B. Tests against reliability during operation

1) Damp heat: 40 °C, 93 % humidity, 96 hrs.;

2) Dry heat: 150°C for 3 - 10 days (depending on the specific EOCBs application environments);

3) Thermal shock: -50 °C - 125 °C, 100 cycles;

Except for the exposure to dry heat, all other tests have been performed at a professional PCB test house (Microtec GmbH, Stuttgart).

### 4.5.2 Determination of Simulating Aging Time and Samples Sizes

To estimate test time compression and devise test plans that include sample size requirements, both acceleration models and statistical analysis are required.

## A. Determination of simulating aging time

#### 1). Dry Heat Operating Life Acceleration Model

In High-Temperature Operating Life testing, devices are subjected to elevated temperature under bias for an extended period of time. Often, it is assumed that the dominant thermally accelerated failure mechanisms will follow the classical Arrhenius relationship. The traditional dry heat Arrhenius acceleration model is provided in Eqn. 4.14. The Arrhenius function is important. It is not only used in reliability to model temperature-dependent failure-rate mechanisms, but it also

expresses a number of different physical thermodynamic phenomena. In Equation 4.14, we see that this factor is exponentially related to the activation energy. As the name connotes, in the failure process there must be enough thermal energy to be activated and surmount the potential barrier height of value $E_a$. As the temperature increases, it is easier to surmount this barrier and increase the probability of failure in a shorter time period. Thus, the activation energy parameter expresses a characteristic value that can be related to thermally activated failure processes. Each failure process has associated with it a barrier height $E_a$. In practice, when trying to estimate acceleration factor without knowing this value for each potential failure mechanism, a conservative value is used. For example, 0.7 eV is typically used for IC failure mechanisms and appears to be somewhat of an industry standard for conservatively estimating test times. With respect to EOCB products, high temperature stability PDMS (up to 300 °C) is integrated into PCB and obviously the activation energy is not determined by PDMS but its surrounding PCB materials so we will continue to keep the value for calculation of temperature acceleration factor in the model. That is, a low value will overestimate the test times and/or sample sizes needed to meet test objectives.

Obviously, the other important considerations are the actual use and stress temperatures. These estimates may also have errors. For example, to accurately assess time compression in testing, a device's junction temperature rise under bias needs to be taken out.[98]

$$A_T = Exp\{\frac{E_a}{K_B}[\frac{1}{T_{use}} - \frac{1}{T_{stress}}]\} \qquad (4.14)$$
$$Test\ Time = Life\ Time / A_T$$

Notation: $A_T$=Temperature acceleration factor, $T_{stress}$= Test temperature (K), $T_{use}$=Use temperature (K), $E_a$= Activation energy, and KB=8.6173e-5 eV/ °K (Boltzmann's constant).

In terms of the definition for dry heat test to EOCB, test time is 96 hours, test temperature is 150 °C and use temperature is supposed to be 25 °C.

From Eq. 4.14, the acceleration factor is:

$A_T$ = Exp {(0.7 eV/ 8.6173 × 10–5eV/ °K) × [1/(273.15 + 25) –1/(273.15 + 150) °K]} = 3128.99

From Eq. 4.14, the test time of 96 hours can simulate:

Life Time= Test Time × $A_T$ = 96 × 3128.99 = 300,353 hours = 34.3 years.

**2). Temperature-Humidity-Bias (THB) Acceleration Model (Damp heating)**

In THB, test devices are put at elevated temperatures and humidity under bias for an extended period of time. One of the most common THB models used in the industry is a 1989 Peck model shown in Equation 4.15. This includes a relationship between life-and-temperature (Arrhenius model) and life-and-humidity (Peck model), so that the product of the two separable factors yields an overall acceleration factor. When Peck originally proposed this model, he reviewed all published life-in-humidity conditions versus life at 85 °C/ 85% RH for epoxy packages. His results found good agreement with the model. Fitted data found nominal values for Ea to lie between 0.77 and 0.81 and nominal values between 2.5 and 3.0 for m.[98]

Notation: $A_{TH}$ = temperature-humidity acceleration factor, $R_{stress}$=relative humidity of test, $R_{use}$=nominal use relative humidity, and m=humidity constant (To normal IC chip and PCB, it was set to be 2.66. For PDMS is a hydrophobic materials and has a good water resistant properties 2 times more than epoxy applied for packaging in IC chip, in the model we set it to be 5.2.).

$$A_T = Exp\{\frac{E_a}{K_B}[\frac{1}{T_{use}} - \frac{1}{T_{stress}}]\}$$

$$A_H = (\frac{R_{stress}}{R_{use}})^m \qquad (4.15)$$

$$A_{TH} = A_T \cdot A_H$$

$$Test\ Time = Life\ Time / A_{TH}$$

In terms of the definition for damp heat test to EOCB, test time is 96 hours, test temperature and humidity are 40 °C and 93 % RH and use temperature temperature and humidity are 25 °C and 40 % RH.

From Eq. 4.15, The temperature acceleration factor is:

$A_T$ = Exp {(0.7 eV/ 8.6173 × 10–5eV/ °K) × [1/(273.15 + 25) –1/(273.15 + 40) °K]} = 3.69

The humidity acceleration factor is

$A_H = (93\ \%RH/\ 40\ \%RH)^{5.2}$ = 80.43

Therefore, the combined temperature humidity acceleration factor is:

$A_{TH}$ = 80.43 × 3.69= 296.8

From Eq. 4.15, the test time of 96 hours can simulate:

Life Time= Test Time × $A_T$ = 96 × 296.8 = 28,492 hours.

### 3). Temperature Shock Acceleration Model

In Temperature shock, test devices are subjected to a number of cycles of alternate high and low temperature extremes. This cyclic stress produced in temperature shock is related to thermal expansion and contraction undergone in the material. To relate field usage to accelerated test conditions, the most widely used model in industry is the Coffin-Manson model. This is a simple model used for estimating the temperature shock and cycle acceleration factor (see Eq. 4.16).

Reasonably estimating the acceleration factor depends on the failures being caused by fatigue subject to the Coffin-Manson law for cyclic strain versus the number of cycles to failure. Values between 2 to 4 have typically been reported in the literature for K. These values are related to the specific design. A value of 2.5 is commonly used for solder-joint fatigue, while 4 is often reported for IC interconnection failures. The lower value (2.5) is a good value for conservative estimates.

Additionally, for Tg of PDMS in under -50 °C and the decomposition temperature is up to 300 °C, hereby, to EOCB products K we choose 3.5 for estimation of the life time.[98]

$$A_{TS} = \left(\frac{N_{use}}{R_{stress}}\right) = \left(\frac{\Delta T_{stress}}{\Delta T_{use}}\right)^{K} \quad (4.16)$$

Notation: Test: -50 to 125 °C, Nominal= -5 °C to 25 °C and K= 3.5,

$A_{TS}$ = $(T_{Stress}/ T_{Use})^K$ = (175 °C/ 30 °C)$^{3.8}$= 479.4, and tem times cycles for one day. Test cycles are 100 and thus for 10 days. So the simulating aging time is 4794 days and about 13 years.

## B. Determination of samples sizes

There are numerous types of accelerated tests. Any test that in some way accelerates environmental use conditions is an accelerated test. Two of the most common types of accelerated tests used in industry are catastrophic and

failure-free testing. In a catastrophic accelerated test, a frequent objective is to estimate the failure rate at a use condition. DMT is based on failure-free testing. The main objective of a DMT (Design Maturity Testing) test is to determine whether a design will meet its reliability objective at a certain level of confidence. This requires that a statistically significant sample size be tested in a number of different stress tests. However, at this point, we would like to illustrate how to conservatively plan a DMT to demonstrate that a particular reliability objective can be met.

In the part, it will plan accelerated tests for a failure-free DMT to demonstrate that EOCB will meet its reliability objective of 400 FITs (Failure in Time, one FIT is equal to one device failure in $10^9$ device-hours of operation) at the 90 percent confidence level. To estimate the sample size required to show that this component is failure-free of any dry heat, damp heat and temperature shock type failure modes. The acceleration factors found above will be used for design.

In the design, we assume that each test will check for different failure modes. This means that each test is allocated a portion of the failure rate. One allocation plan is assigned, where damp heat-, temperature shock-, and dry heat-type failure modes were assigned 50 percent, 20 percent, and 30 percent, respectively, of the total reliability. Using this plan, the 400 FITs are broken up with 200, 80, and 120 FITs to THB, TC, and HTOL tests, respectively. At this point, a single-sided chi-square estimate for sample-size planning can be used.

Once reliability objectives are established, sample sizes can be planned with statistical confidence. To determine a statistical sample size to meet a particular reliability objective at a specific confidence level, it is common to use a chi-square, $c^2$, confidence estimate, given by (See eq. 4.17).[98]

$$N = \frac{c^2(g, 2Y + 2)}{2\bar{l}At} \quad (4.17)$$

Where, N = the sample size, $l$ = the upper-bound or failure-rate objective, Y = the number of failures (nominally zero), t = the total test time, A = the estimated test/failure mode acceleration factor, and $g$ = the confidence level (nominally 90 %).

For example, the Thermal Shock values are:

Y=0 Faliures, $c^2$(90 %, 2) = 4.605, $l$ = 120 FITs = 1.2 e-7 failure/ hour, A = 479.4 (from calculation on Temperature Shock Acceleration Model) and t = 10 cycles × 24 hours = 240 equivalent test hours.

Thus, N = 4.605/ (2 × 0.8 e-7 × 479.4 × 240) = 251 waveguides = 21 EOCB (For in terms of our mould, every EOCB will include 12 waveguides)

Using this same approach for the other tests, the results are summarized in Table 4.8.

In order to check the influence of the PCB carrier materials on the optical waveguide loss, samples with and without different carrier materials have been prepared. About in terms of reliability objective of 400 FITs and defined minimum sample sizes, samples based on etched FR4, Kapton and copper coated FR4 substrates and respective SAPs are fabricated in terms of the procedure shown schematically in Fig.4.21. The sample sizes for lamination simulating and solder floating are both set to be 5 EOCBs, i.e. in the level of 60 waveguides for the two simulating temperatures are both lower than the decomposition temperature of PDMS and the lasting times are very short as well. The thickness of the PDMS waveguide layer is about 200 μm resulting in a total sample thickness (including the two PCB carrier layers) of about 400 - 600 μm. The dimensions of the samples prepared for the environmental tests are 10 cm × 1 cm, each carrying 12 parallel straight waveguides.

**Table 4.8** *Minimum sample sizes for EOCB environmental stability tests*

| ***Accelerated Test*** | ***Acceleration Factor*** | ***Test Time (hours)*** | ***FITs*** | ***Sample Size*** |
|---|---|---|---|---|
| ***Dry heat*** | 3128.99 | 96 | 120 | 6 |
| ***Damp heat*** | 296.8 | 96 | 200 | 34 |
| ***Temperature shock (100 cycles)*** | 479.4 | 240 | 80 | 21 |
| ***Lamination*** | N.A | N.A | N.A | 5 |
| ***Soldering floating*** | N.A | N.A | N.A | 5 |

## 4.5.3 Optical Stability of EOCBs

The influence of all environmental tests on refractive indices (measured at 589 nm) of PDMS core and cladding is illustrates in Fig. 4.29 and three test procedures (damp heat treatment, thermal shock, and soldering float) on the optical waveguide

loss is summarized in Fig. 4.30 and results after simulating lamination has been illustrated in Fig. 4.27. For evaluation, 12 waveguides on each sample have been measured at 850 nm wavelength before and after each test. The tests have been performed with PDMS waveguide samples laminated between three different PCB carriers: uncoated FR4, copper coated FR4, and Kapton.

The results show that damp heat has no significant influence on the loss which is expected because of the good water resistant properties of PDMS material. Similar insignificant changes of the loss figures are observed after thermal shock treatments. This is explained by the high mechanical flexibility of the PDMS material. The influence of dry heat on the waveguide loss is documented in Fig. 4.31. The motivation for testing the waveguide samples against dry heat results from general PCB-requirements concerning their long-term durability at high-temperature operation conditions. Figure 4.31 shows the resulting waveguide loss figures before and after dry heat exposure. The waveguide loss remains stable up to about 4 days, after 5 days a loss increase of about 0.02 dB/cm is observed and after 10 days the total loss increase is about 0.03 dB/cm. We conclude that the waveguide transmission loss is quite sensitive to long time dry heat exposure (150 °C, 10 days). However, even at these strongest test conditions, the total waveguide transmission loss remains below 0.1 dB/cm which is a required target for most of the optical interconnect applications.

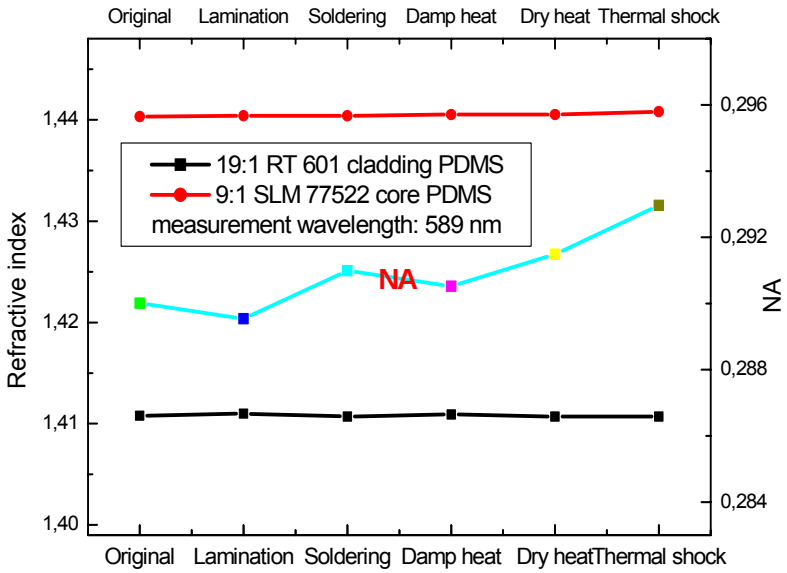

**Figure 4.29** *Influence of different environmental conditions on optical wavguide materials refractive indices and NA*

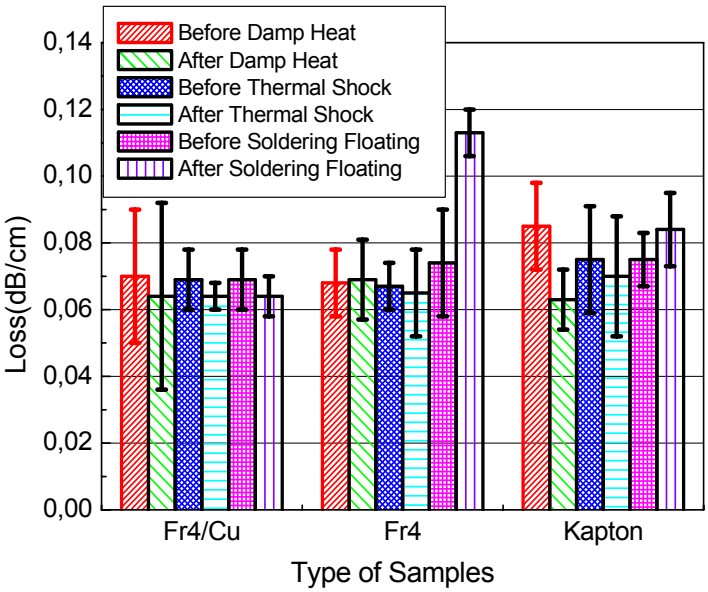


**Figure 4.30** *Influence of different environmental conditions and different PCB-carrier materials on optical wavguide loss*

## 4.5.4 Mechanical Stability of EOCBs

The mechanical stability of fabricated EOCBs depends in a crucial way on the interfacial strength between the optical PDMS layer and the PCBs. If not strong enough, thermal stress resulting from CTE (Coefficient of Thermal Expansion) and Young's modulus mismatch will cause delamination and therefore damage. We have tested the mechanical stability of PDMS layers embedded between two copper coated FR4 laminates against the environmental test conditions indicated above by using a pull-off test described in detail in chapter 4.4.3. The obtained results for the maximum mechanical strength are shown in Table 4.9. By comparing the achieved values with the measured stability limit of pure PDMS (1.35 ± 0.33 MPa) it is clear that the mechanical stability limit of the prepared samples is determined by the intrinsic material stability of the PDMS layer and not by the interface properties. Similar results are obtained for laminates made from Kapton, uncoated FR4 and ED copper.

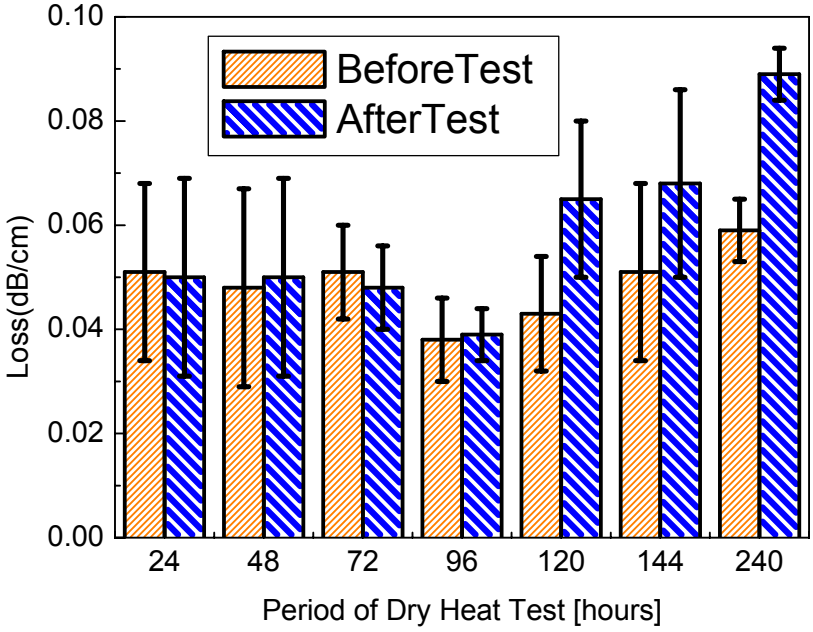


**Figure 4.31** *Influence of dry heat treatment on optical waveguide loss*

**Table 4.9** *Maximum mechanical strength after different environmental tests*

| ***Test item*** | ***Max. pull strength of laminate (MPa)*** |
|---|---|
| ***70 °C 2hrs curing*** | 1.35 ± 0.33 |
| ***After lamination*** | 1.44 ± 0.29 |
| ***After thermal shock*** | 1.41 ± 0.28 |
| ***After damp heating*** | 1.37 ± 0.32 |
| ***After Dry heat*** | 1.37 ± 0.31 |
| ***After soldering float*** | 1.42 ± 0.28 |

## 4.6 Summary of results of the chapter

In the chapter, a novel self-packaging method of PDMS based optical waveguide layers laminated to standard PCB carrier materials has been experimentally verified with identified optimum bonding conditions. The mechanical stability of the fabricated EOCBs is limited not by the interfacial bonding strength between PDMS and PCBs, but by the intrinsic mechanical stability. Reasonable environmental test procedures to check the optical and mechanical stability performances of EOCBs have been defined and implemented to PDMS-waveguide layer based EOCBs. Except the good mechanical stability the packaged EOCBs exhibit low and stable optical loss values (<0.1 dB/cm) even at extreme environmental conditions.